Structural investigation of masonry arch bridges using various non-linear finite element models

Authors

Serkan Tapkın[a], Emre Tercan[b], Siphesihle Mpho Motsa[c,*,1], Georgios Drosopoulos[d], Maria Stavroulaki[e], Emmanuel Maravelakis[f], Georgios Stavroulakis[g]

[a] Bayburt University, Faculty of Engineering, Department of Civil Engineering, 69010, Bayburt, Turkey.
Academic position or professional affiliations: Professor, Dr
Email: serkantapkin@bayburt.edu.tr
ORCID: 0000-0003-1417-9972

[b] General Directorate of Highways, 13th Region, Department of Survey, Project and Environment, 07090, Antalya, Turkey.
Academic position or professional affiliations: Geomatics Engineer (PhD)
Email: etercan87@gmail.com
ORCID: 0000-0001-6309-1083

[c] Discipline of Civil Engineering, Structural Engineering and Computational Mechanics Group, University of KwaZulu-Natal, Durban, South Africa.
Academic position or professional affiliations: MSc, BSc
Email:214580281@stu.ukzn.ac.za
ORCID: 0000-0003-4990-5225

[d] Discipline of Civil Engineering, School of Engineering, University of Central Lancashire, Preston, United Kingdom
Discipline of Civil Engineering, Structural Engineering and Computational Mechanics Group, University of KwaZulu-Natal, Durban, South Africa.
Academic position or professional affiliations: Lecturer, Dr
Email: gdrosopoulos@uclan.ac.uk
ORCID: 0000-0002-4252-6321

[e] Faculty of Architecture, Applied Mechanics Laboratory, Technical University of Crete, Chania, Crete, Greece
Academic position or professional affiliations: Associate Professor, Dr
Email: mstavr@mred.tuc.gr
ORCID: 0000-0003-0882-5763

[f] Department of Electronic Engineering, Hellenic Mediterranean University, Greece
Academic position or professional affiliations: Associate Professor, Dr
Email: marvel@hmu.gr

[g] School of Production Engineering and Management, Institute of Computational Mechanics and Optimization, Technical University of Crete, Chania, Crete, Greece

Academic position or professional affiliations: Professor, Dr

Email: gestavr@dpem.tuc.gr

ORCID: 0000-0001-9199-2110

* Corresponding author at: Discipline of Civil Engineering, Structural Engineering and Computational Mechanics Group, University of KwaZulu-Natal, Durban, South Africa.

Email:214580281@stu.ukzn.ac.za

[1] URL: https://ukzn.ac.za

Abstract

In the present article, the structural behaviour of a masonry arch bridge in Turkey is investigated. An analytical study has been conducted to provide the geometry of the structure, using laser scanning. A point cloud describing the geometry is obtained and properly transformed into a format, which is appropriate for structural analysis software (CAE). Then, a number of non-linear finite element models is developed, to simulate its structural response. Goal of the article is to highlight the influence of both continuum and discrete approaches and related constitutive laws, on the response of the bridge. Thus, continuum damage laws and a discrete model consisting of unilateral contact-friction interfaces, have been developed. Different load cases are tested and comparison between the results obtained from the different approaches is considered. The failure mechanisms and the ultimate strengths are derived and core points of the used models are highlighted. From the output of this work, it is shown how the different failure models predict the behaviour of the masonry arches. It is also shown that the three-hinge mechanism, which has been depicted in classical studies for single-span arch masonry bridges under a horizontal settlement of supports, may also be obtained for multi-arch bridges. Similarly, downward, vertical settlement of supports may result in the development of two hinges, as in single-span arches. The beneficial influence of the backfill in limiting the failure in the arch, is finally addressed in the article.

Keywords: Masonry arch bridge, Terrestrial laser scanning, Unilateral contact-friction, Continuum damage model, discrete element method

Introduction

Masonry arch bridges are among the oldest structures, which have survived for thousands of years (Sevim et al. 2011). They are found in various sizes and configurations and their aesthetic details vary significantly (Catalan and Aldea 2007). Masonry arch bridges play a vital role in the cultural heritage of several countries, highlighting the need to be preserved. Research conducted by Van Beek (1987) and Campbell and Tutton (2013) in Lower Egypt, Iran, the Eastern Mediterranean region and Mesopotamia showed that the earliest masonry arch structures (about 5 000 years old) were made up of sun-dried, mud bricks.

A thorough understanding of the structural behaviour of masonry arch bridges is of crucial importance, towards their restoration and preservation. Ageing as well as different loads due to earthquakes, settlement of supports and vehicles, have an increased impact on their structural condition, causing significant damage and/or collapse of these structures. Hence, their conservation and preservation are of paramount importance. The process of structural restoration includes (a) visual assessment of the structure, (b) material testing by adopting, for instance, non-destructive tests for the constituent materials, (c) understanding of the original design and the structural capabilities by developing numerical models, and (d) implementing the actual restoration of the different elements of the structure after the previous steps have been considered.

Most of the old masonry arch bridges have sustained some form of damage over the years while in service. Some of the common structural problems that they experience, which can lead to failure and collapse, are provided below: (a) deterioration of the masonry material due to thermal effects, moisture, or chemical actions, (b) damage of the arch barrel due to

ring-separation, arch barrel distortion and cracking which is a result of longitudinal shear or tensile failure (Ford et al. 2003; Melbourne 1991), (c) failure of the foundation which is mainly caused by settlement of supports (Ashurst 1992), and (d) vehicle collision which can interact with abutments, arch barrels or piers (Melbourne et al. 2006; Wilmers 2012). It can be noticed that some of these defects take place simultaneously.

In recent years, several studies have been conducted to evaluate the structural behaviour of masonry arch bridges and improve their ultimate strength. Some of the recognised techniques used in the assessment of masonry arch bridge include, (a) the Military Engineering Experimental Establishment (MEXE), a semi-empirical method which is based on elastic analysis and it only considers the independent strength of the arch barrel (Hughes et al. 1997), (b) the collapse mechanism method, which uses simple equilibrium calculations based on the assumption that the collapse of the arch barrel takes place due to the formation of a four-hinge mechanism (Hughes et al. 2002; Page 1993), and (c) the finite element method which relies on the development of a computational, structural, model, considering the influence of each element of the bridge (arch barrel, spandrel walls, wing walls, fill and parapets) (Crisfield 1985; Towler 1985). This method is widely recognised over the years as an efficient and effective approach which can be adopted for the structural assessment of old masonry structures (Armesto et al. 2010; Ataei et al. 2016; Conde et al. 2017; Domede et al. 2013; Lubowiecka et al. 2009; Sevim et al. 2011).

In the structural investigation of masonry arches, it has been noticed that the geometry of the structure plays a vital role on its structural integrity and a change of the geometry in respect to the original one, can result in excessive deformation leading to collapse (Guastavino and Moreno 2006). In Armesto et al. (2010) and Conde et al. (2017) , finite

element models of masonry arch bridges have been developed, using terrestrial laser scanning technology to obtain the real, exact geometry of the structure. In particular, a deformation analysis of Segura Roman Bridge is performed in Armesto et al. (2010), by creating a 3D geometry from unstructured point clouds, collected from 6 different positions around the bridge. A non-parametric algorithm is also proposed, which generates a smooth 3D surface based on local bivariate kernel smoother, allowing for the estimation of cross-sections without the need of any prior parametric shape. In Conde et al. (2017), 3D finite element models of the Vilanova masonry arch bridge are developed, based on a comprehensive field survey, which is conducted by adopting fully non-destructive testing techniques like laser scanning, ground penetration radar, sonic tests and ambient vibration tests. As part of the study, 2D limit state analysis is performed on one of the arches of the bridge, to depict the effect of the live load and to determine the impact of the four-hinge failure mechanism, which was initially presented in Heyman (1982), on the structural response of the arch.

In Ataei et al. (2016), a load capacity assessment is conducted on an 80 years old masonry arch bridge, consisting of 10 arch spans. Finite element analysis and limit analysis models using the RING software (RING 2021), are developed for the arch of the main span of the bridge, with a length 40 m and height 30 m. Continuum numerical models have been used, allowing for the estimation of deformations with a high precision (0.01mm). The study showed that the bridge can still be in service even when the axle load is increased from 200 kN to 250 kN.

In Lubowiecka et al. (2009) and Sevim et al. (2011) studies on masonry arch bridges are conducted, by introducing modal analysis to calibrate the developed non-linear finite

element models. In particular, in Lubowiecka et al. (2009) it is observed that the value of the Young's modulus is vital for the natural frequencies of the structure, noticing that a similar observation is derived in Motsa et al. (2020). In Sevim et al. (2011), a time-history ground motion acceleration of a 0.515g is applied on the calibrated finite element model, resulting in acceptable stress limits for the masonry stones and a maximum displacement of 8.2 mm developed at the middle region of the span.

In Domede et al. (2013) a 3D finite element model is developed for a 3-span masonry arch bridge. In an effort to reproduce the failure cracks which are really present on the structure, a settlement of the middle support is assigned. On the damaged model of the bridge an increasing train load is applied, resulting in a failure load of 25MN. The results of the study show that the safety margin between failure load and service load is very high.

Some more recent articles can also be identified, highlighting significant aspects of the structural response of masonry arches. In (Sarhosis et al. 2016) a literature review is provided, on experimental investigations and assessment methods for masonry arch bridges. In (Pulatsu et al. 2019) masonry arch bridge models are developed using a mixed discrete-continuum approach. Aim of this study is to depict the influence of the soil backfill and of the spandrel walls on the mechanical response. In (Casapulla et al. 2019) and in (Mousavian and Casapulla 2020), a digital tool is proposed, for the design of stable semi-circular masonry arches consisting of interlocking blocks. To increase the sliding resistance between the blocks comparing to conventional blocks, interlocking connectors are introduced in the analysis. In (Zampieri et al. 2015) a kinematic analysis process is developed, to address the transverse seismic capacity and provide the limit horizontal load of multi-span masonry bridges with slender piers. In (Gönen and Soyöz 2021) different

numerical methods are investigated, including non-linear static and dynamic finite element models, towards the evaluation of the seismic response of masonry arch bridges.

In this paper, the structural investigation of a masonry arch bridge, namely the Dağarcık bridge located in Turkey, is presented. By using two types of computational models, adopting a discrete and a continuum mechanical description respectively, into a three-span arch, the work focuses on studying the development of failure patterns, which are previously derived in single-span arches. These patterns involve the development of hinges representing cross-section failure, when settlement of supports, both horizontal and vertical, arise. Since this loading type can result in the total collapse of masonry arches, the investigation of the phenomenon for multi-span arches, provides an innovative aspect to the current investigation. It is actually proved, that hinge mechanisms of single-span arches due to settlement of supports, may also arise in multi-span arches.

From another point of view, the present work provides an insight on two types of constitutive descriptions, focusing on a discrete and a continuum approach. Both concepts have been used in old and current research on masonry arches. Hence, it appears the need for a holistic investigation of their mechanical, ultimate response, using the two approaches as well as a combination of them. In the article, details of the used parameters within the two descriptions are provided and important points are introduced, highlighting advantages and disadvantages of them.

First, 3D laser scanning is used to represent the geometry of the bridge, in the form of a point cloud. This is converted into a 3D solid geometry using AutoCAD. Then, a series of non-destructive tests are conducted on the masonry stones of the bridge, to provide their mechanical properties. Finally, a number of non-linear finite element models are

developed, adopting both discrete and continuum mechanical laws. The discrete models incorporate unilateral contact-friction interfaces between the masonry stones. The continuum models include a smear crack and a damage plasticity law, applied on the masonry arch to represent failure. The soil backfill which is found above the arches is also introduced in some of the models and its influence on the mechanical response of the structure is highlighted. The developed numerical models are used to evaluate the structural response of the masonry bridge under various load cases.

Research aim

The goal of this study is to investigate the structural behaviour of a masonry arch bridge and provide a further insight on mechanical laws which can be used for the task. The developed numerical models are applied to the Dağarcık bridge, which is located in Turkey. The structural investigation of this historically and architecturally important monument, is conducted by considering a combination of non-destructive tests and numerical (finite element) analysis. First, a 3D laser scan of the masonry structure is implemented, where 91 360 850 cloud points are collected from 9 scanning position stations around the bridge. Then, non-linear finite element analysis takes place, adopting either a discrete or a continuum approach. According to the discrete approach, unilateral contact-friction interfaces are introduced between the masonry stones, to simulate the mortar joints. Opening and/or sliding of those interfaces indicates damage. For the continuum approach, two failure laws initially adopted for concrete, are applied to the arch. Discrete models incorporating the continuum laws are also developed, to offer a further insight to the mechanical response. Opening or sliding of the interfaces and compressive failure of the

arch can be depicted by this combination of discrete and continuum laws. The mechanical properties of the masonry stones are obtained from non-destructive tests and the literature.

Figures 1a and 1b show some of the inherited features of the bridge under investigation, which have been simulated by the numerical models through the use of the point cloud. Further defects like the slight settlement of the supports, which are sometimes difficult to be identified by a physical inspection, are also simulated by the developed numerical models. It is noted that the overall concept presented in this study, adopting laser scanning of a masonry arch and structural analysis using various non-linear finite element models with different constitutive descriptions, can also be applied for other masonry structures.

Description of the Dağarcık bridge

The Dağarcık bridge is located in the Onaç River, found within the boundaries of Dağarcık village, located 22 km southeast of Burdur city centre and 11 km north west of Bucak District in Turkey. There is no inscription on the Dağarcık Bridge indicating the date of construction or renovation. This masonry arch bridge is of great historical and architectural importance, since it is believed it was built during the Roman era. The bridge has been registered as "Real Estate Cultural Asset required to be protected" by the decision of the Antalya Cultural and Natural Assets Protection Regional Board on 23.01.2015 (GDH 2017).

The Dağarcık bridge consists of 3 masonry arches. Details for the geometry of the bridge are found in Figure 2a. In particular, from the downstream views of the structure shown in Figures 2a, 2b and the upstream view shown in Figure 2c, it is obtained that the first (left) arch has a length of 3.28m and a height of 2.44 m. This arch consists of five stone sequences

up to keystone. The middle arch has a length of 3.20 m, a height of 2.67 m and consists of six stone sequences up to keystone. The last arch has a length of 2.93 m a height of 2.54 m and consists of five stone sequences up to keystone (GDH 2017).

The masonry stones of the arch are made of travertine. Their mechanical properties were obtained from experimental investigation of the material in-situ and literature studies presented in (GDH 2017). In this article, the mortar between the stones has not been considered due to its poor condition.

The proposed structural models

Adopted constitutive descriptions

Six non-linear finite element models have been developed in this study, to provide a holistic insight of the structural response for the considered masonry arch bridge, emphasizing in potential collapse mechanisms. The first, is a discrete model consisting of unilateral contact-friction interfaces, used to simulate potential failure due to opening/sliding between the stones of the arch. Due to the presence of the contact laws assigned between the stones, the model is non-linear. Linear elastic material properties are also considered for the stones.

The second model uses a continuum, smeared cracking constitutive law to simulate compressive and tensile failure of the arch. This law is appropriate for monotonic loading, at low confining pressures.

An alternative, concrete damage plasticity, continuum constitutive description is considered in a third model. This is appropriate for the simulation of failure on quasi-brittle

materials and may also be used when cyclic loads are considered. Damage variables are introduced in the material law, to capture failure under tension and compression.

The fourth model, uses the discrete approach with the unilateral contact-friction interfaces but is also enriched with the continuum concrete smeared cracking model. The fifth model adopts the discrete approach, enriched by the damage plasticity model.

A final, sixth model is developed, incorporating the backfill, soil material above the arch, in the analysis. A Mohr-Coulomb failure law is adopted for the fill. The arch is this case, is simulated using the continuum concrete damage plasticity law.

It should be noted that the discrete models are useful in representing hinged failure mechanisms, after opening of the interfaces occurs. The continuum models, can depict the type of failure experienced by the structure, either compressive or tensile. Combining the discrete and the continuum description in one model, may lead to both opening of the interfaces (hinges) and compressive (or tensile) failure of the material (if any). A list of the developed models is found in Table 1.

General description of the model

FARO Focus3D X130 terrestrial laser scanner was used in order to create an accurate 3D model of point cloud representing the geometry of the arch bridge. User requirements for the level of detail, the colour, the selection of the coordinate system of reference and the type of the 3D product (Maravelakis et al. 2013) were defined during the initial planning of the project. The produced point cloud was then processed in AutoCAD and a total of 200 individual building blocks of the arch bridge were manually extracted using selected points and profiles from the point cloud.

The geometry created was exported as a STEP file and was imported on Abaqus 6.12-3 (Hibbitt et al. 2012) for the creation of the finite element models. To simulate the different loading cases that the bridge may experience, both fixed supports and settlement of supports have been considered as the boundary conditions at the bottom side of the structure.

The developed models consist of 58 320 three-dimensional finite elements used to simulate the three arches, Figure 3a. A closer view of the mesh density is shown on Figure 3b. The finite elements are 8-node solid elements (hexahedrons) with three displacement degrees of freedom at each node. In Figures 3c and 3d the mesh of the structure is provided, when the backfill soil material above the arch is included in the simulation.

Hinge-mechanism

The classical collapse mechanism of arch bridges, which was presented in Heyman (1982), has been adopted for the determination of the load carrying capacity of stone arch bridges in previous studies, for instance in (Drosopoulos et al. 2008). This technique uses the funicular polygon as the fundamental tool of analysing arches and is based on the estimation of the thrust line carrying the load on the arches. For a rectangular section of stones (voussoirs), the thrust line lies within the middle third 'core' of the section (Heyman 1982).

A hinge is formed when the thrust line in a cross-section is adjacent to the ring of the arch, at an eccentricity e of the normal force P, from the centre line of the arch. The resultant bending moment M is equal to Pe and is developed around the centre line of the arch, assuming the arch is unreinforced and therefore, it does not develop any tensile strength.

A single-span arch with two fixed supports has a determinacy degree of three. When three hinges are developed, the structure becomes statically determinate. Then, the development of a fourth hinge will turn the structure into a mechanism, leading to collapse. This collapse mechanism is common in unreinforced masonry arch bridges, with a vertical load acting at one quarter of the span of the arch. According to Heyman (1982), this is the worst load position, resulting in the lowest resistance.

In the present study, a vertical load is applied at one quarter of one of the spans of the bridge acting together with the self-weight of the structure. Compressive failure is not usually expected according to (Heyman 1982), since the developed compressive stresses are generally low. However, the continuum laws which have been used, can capture also this failure type.

Another outcome of the classical studies presented in (Heyman 1982), is the description of the structural response of arches, when settlement of supports takes place. It was mentioned in these studies that if the abutments spread for a reason, ‘‘the arch could accommodate itself to the increased span by forming three hinges, one at the crown in the extrados, and one at each abutment in the intrados’’. In the same studies it was also claimed that if the abutments are too close, ‘‘three hinges have again been formed to accommodate the decreased span, one at the crown in the intrados and one at each abutment in the extrados”. In (Drosopoulos et al. 2008) these conclusions were verified using non-linear finite element models, in single span, two-dimensional arches. Among the aims of the present study, is to highlight the validity of these conclusions, for multi-span arches.

The ultimate behaviour and collapse prediction within finite element analysis

In the framework of finite element analysis for masonry arch bridges, the ultimate strength of the bridge is defined as the point preceding collapse of the structure. When the structure is close to reach its ultimate strength, the analysis becomes unstable due to the introduction of at least one zero eigenvalue on the tangential stiffness matrix. When the ultimate strength of the structure is finally reached, the analysis is terminated.

In the framework of finite element analysis, the force-displacement diagram obtained at the end of the simulation, is used to determine when the structure is close to collapse, as depicted by the end of the graph.

Material properties using the concrete smeared cracking and the damage plasticity model

A concrete smeared crack damage model, as well as a concrete damage plasticity model, are adopted in the study to consider the compressive and tensile failure of the masonry arch. The smeared crack model allows for the simulation of brittle materials, like concrete and masonry by incorporating the uniaxial tensile and compression behaviour. According to this model, cracking is assumed to occur when the stress reaches a critical failure surface, provided by the relationship between the equivalent pressure stress and the Mises equivalent deviatoric stress.

In the framework of this model, no individual "macro" cracks are developed. In addition, the compressive response of the material is modelled by an elastic-plastic theory. The post-failure behaviour of the damaged material is modelled using a tension stiffening law and the corresponding stress–displacement diagram.

The second continuum approach, introduces the concrete damage plasticity law. This is appropriate for quasi-brittle structures, for instance masonry and concrete, subjected to monotonic or cyclic actions. The main two failure mechanisms, which can be depicted by this law, are tensile cracking and compressive crushing. During unloading the elastic stiffness of the material is considered damaged. This is depicted using two damage variables, one for tension and another for compression, both introduced in the model as functions of the plastic strains. These damage variables take values from zero, representing the undamaged material, to one, depicting total loss of strength. If the initial elastic stiffness of the material is E_0, d_t and d_c are the tensile and compressive damage variables, respectively, then the stress-strain relations under uniaxial tension and compression loading are provided by the following equations:

$$\sigma_t = (1 - d_t)E_0\left(\varepsilon^t - \varepsilon_{pl}^t\right) \quad (1)$$

$$\sigma_c = (1 - d_c)E_0\left(\varepsilon^c - \varepsilon_{pl}^c\right) \quad (2)$$

In Tables 2, 3 and in Figures 4, 5 below, are provided all the material parameters which are used in these two constitutive descriptions. In addition, for all material laws, the Young's modulus, Poisson's ratio and density values shown in Table 4, are adopted. These correspond to the building material used to make the arch bridge, which is travertine (Erdoğan 2011; GDH 2017). The compressive strength of the travertine stone is 70 MPa and the tensile strength is approximately 10% of the compressive strength, 7MPa. This is mentioned in *TS EN 1996-1-1 + A1 Eurocode 6 - Design of masonry structures - Part 1-1: General rules for reinforced and unreinforced masonry structures*, which is one of the codes to design arch bridges (CEN 2005; GDH 2017).

For the models which incorporate the backfill soil material which is found above the arch, a Mohr-Coulomb failure law is used, to simulate damage on the fill. In Table 5, the adopted parameters for this law are given.

Discrete model for the arches

To simulate the contact conditions between each stone, principles taken from contact mechanics have been adopted. For a discrete structure, these relations are written for every point of a unilateral boundary or interface. In the following equations, u is the single degree of freedom and g represents the initial opening between the contacting bodies.

$$h = u - g \leq 0 \Longrightarrow h \leq 0 \qquad (3)$$

$$-t^n \geq 0 \qquad (4)$$

$$t^n(u - g) = 0 \qquad (5)$$

The behaviour in the tangential direction between the stone interfaces, is defined by a static version of the Coulomb friction model. Two contacting surfaces start sliding when the shear stress in the interface reaches a critical value equal to:

$$t^t = \tau_{cr} = \pm\mu|t^n| \qquad (6)$$

where t^t and t^n are the shear stress and the contact pressure at a given point of the contacting surfaces respectively and μ is the friction coefficient. There are two possible directions of sliding along an interface, so t^t can be positive or negative depending on that direction. Furthermore, there is no sliding if $|t^t| < \mu|t^n|$ (stick conditions). The sliding rule can be summarized by the following relations, where u_t is the displacement (sliding) in the tangential direction of an interface:

$$|t^t| < \mu|t^n| \longrightarrow u_t = 0\ (no\ sliding) \quad (7a)$$

$$t^t = \mu|t^n| \longrightarrow u_t \geq 0\ (sliding\ in\ one\ diretion) \quad (7b)$$

$$t^t = -\mu|t^n| \longrightarrow u_t \leq 0\ (sliding\ in\ the\ opposite\ direction) \quad (7c)$$

The Lagrange multiplier method is used to incorporate in the equilibrium equations, the unilateral contact-friction equations. Moreover, a friction coefficient equal to 0.5 is adopted in this study (Melbourne and Gilbert 1995). For the continuum models, a tie-constraint condition is considered for the interfaces between the masonry stones. This prevents sliding and opening at the interfaces, in all directions.

Results and discussions

Load cases

In the present study, the structural behaviour of a masonry arch bridge is investigated, using different load types and adopting different numerical models to predict the structural response.

The different load types which are implemented, are based on critical load cases, that the bridge is likely to experience in situ. These load cases include loads applied as forces and displacements in the plane, as well as in the out-of-plane direction of the bridge, in different positions. In particular, the following load cases are considered: (a) a vertical load applied at about one quarter of the middle span of the bridge, to determine the ultimate strength, (b) a horizontal, outwards displacement of 100 mm in the plane of the bridge, on both outer supports, representing settlement of supports, (c) a horizontal inwards displacement of 100 mm in the plane of the bridge on both supports (d) 100 mm horizontal displacement of the two internal supports in the direction of the water flow, perpendicular to the plane of the

bridge, (e) a vertical load applied at about one quarter span of the middle span of the bridge with 20 mm displacement of the two internal supports in the direction of the water flow perpendicular to the plane of the bridge, (f) 100 mm vertical displacement of the two internal supports in the downward direction, (g) a vertical load applied at about one quarter span of the middle span of the bridge with 20 mm vertical displacement of the two internal supports in the downward direction. The first four load cases are also considered for the model with the backfill above the arch. It must be noted that the vertical load is equally distributed into 5 points along the width of the bridge, to minimize the effects of localized failure. All load cases are provided in Table 6.

In the developed numerical models, two steps are considered. The first, is a dynamic implicit analysis step, in a quasi-static framework, which introduces a gravity load (self-weight of the structure) of 9.81 m/s^2. When a general static analysis was considered in the first step, numerical singularities did not allow the model to reach convergence due to the extensive number of unilateral contact-friction interfaces, which are used to simulate the contact conditions between each stone. This numerical instability was attributed to multiple micro openings/closures between stone interfaces, resulting in unstable stiffness matrices. To overcome this problem, the mentioned dynamic implicit analysis, in a quasi-static framework, was used. This introduced the mass stiffness in the equilibrium equations, resulting in more stable stiffness matrix. Then, a second step is applied, with the particular loading, which is described above.

Discrete models with and without concrete plasticity laws

Results of the three discrete models with the linear elastic, smeared cracking and damage plasticity constitutive description, are presented in this section for the different load cases.

Within the first load case, a vertical load is applied at about one quarter of the middle span, to determine the ultimate strength of the structure. Results indicate that a local sliding of the stones near the point of application of the vertical force, is obtained from the three discrete models. In addition, although the four-hinge mechanism does not clearly appear, two more hinges arise left and right of the point force (extrados opening). The fourth hinge, that would normally appear close to the left support of the loaded arch in the classical four-hinge mechanism, only slightly emerges in the present models, but cannot be depicted in the image.

This is shown for the pure discrete model in Figures 6a and 6b, where a scale factor has been used to magnify the obtained displacements and better highlight the hinges. A similar result is obtained from the discrete models which use the plasticity laws, as depicted in Figure 7, noticing also that for these models a local failure of the material near the point of application of the vertical load also arises.

From these figures it is obtained that the pure discrete model results in higher displacements (Figure 6b), comparing to the ones which use the plasticity laws (Figure 7). This observation, highlighting a more brittle behaviour due to usage of the plasticity laws, is also derived for the majority of the presented results.

Next, horizontal, outward, in-plane settlements of the supports of the outer arches, have been applied to the three discrete models. Figure 8 shows the plot of the final displacements for outward settlement of 100mm in both outer supports, which could arise due to erosion of the riverbed, riverbank and the soil in the vicinity of the supports. It is clearly shown in this figure, that the three-hinge mechanism described in the classical studies of (Heyman 1982) for similar settlement of supports, also arises here for the three-span arch. In

particular, similar to (Heyman 1982), one hinge appears at the crown at the extrados of the arches (opening at the intrados), and one at each support in the intrados (opening at the extrados). For the right outer arch, a sliding instead of an opening arises, at the position where the right hinge would appear. It is noted that the same mechanism appears for the three discrete models, without any material failure (except the hinges).

The plot of the final displacements of the structure when an inward movement of 100 mm is considered for the outer supports, is shown in Figure 9. According to this figure, sliding arises in this case, at the two supports of the bridge. Thus, contrary to the case of outward settlement of supports, where a three-hinge mechanism appeared, for inward settlement the mechanism changes to sliding failure. For the discrete models with the plasticity laws, no failure on the material arises.

In Figure 10 the plot of the final displacements of the bridge is shown, when an out-of-plane settlement of 100 mm occurs on the two internal supports, in the direction of the water flow. Since the outer supports are fixed, the structure develops an out of plane bending response, resulting in the opening of hinges at the two outer arches, as shown in Figure 10. These hinges are developed at the top of the two outer arches as well as at the supports of the right arch. The middle arch does not develop any particular damage.

An additional analysis has been conducted, combining the out of plane settlement of the inner supports and the vertical point force at the one quarter of the span of the middle arch. Results in this case resemble the ones presented in Figures 6 and 7 and thus, they mainly involve hinge opening at the middle arch, where the vertical load is applied.

The plot of the maximum principal stresses is provided in Figure 11, when a downward settlement of 100 mm of the two internal supports is considered. According to this figure,

two hinges open in the outer arches, one closer to each inner support (opening intrados) and another closer to the outer support (opening extrados). It is also noted that the position of the hinge closer to the inner support is different in the two outer arches. A similar hinge-mechanism for downward settlement of supports is derived in (Drosopoulos et al. 2008) for two-dimensional, single-arch bridges.

The plot of the maximum principal stresses is shown in Figure 12, for a final load case of a vertical load equal to 100 kN applied at about one quarter of the span of the middle span of the bridge together with a 20 mm downwards movement of the two internal supports. Contrary to the case of downward settlement of support without any vertical load shown in Figure 11, the two hinges are not developed in the outer arches. Instead, only one hinge is developed in the outer left arch, while no hinge appears in the outer right arch, as depicted in Figure 12. Hinges arise in the middle arch, due to the vertical point force.

Continuum models

The failure of the bridge is shown in this section, by using the plastic strain distribution, arising when the different load cases are applied. Within the continuum models, no opening or sliding between the masonry bricks can be depicted. Instead, material failure may be derived, due to compressive or tensile response.

Within the first load case, a downward vertical force is applied to the quarter of the span of the middle arch. The model with the smeared cracking constitutive description did not provide any failure mechanism, except local failure near the points of applications of the load. On the contrary, the model with the concrete damage plasticity law resulted in the failure response which is shown in Figure 13. Thus, failure appears in four regions of the

arch. It is noted that the same mechanism arises in single-span arches, according to classical studies (Heyman 1982).

For the outward displacement of the two outer supports, the simulation with the smeared cracking continuum model terminated early, due to convergence issues, arising from the brittle response which is depicted in this constitutive law. On the contrary, the concrete damage plasticity model provided a much-improved convergence response, allowing for the representation of damage. The three-hinge mechanism, which is derived in the classical studies of (Heyman 1982) and is also obtained from the discrete models of the previous section, appears in this case too, as shown in Figure 14. According to this figure, the hinge at the crown is in the same position with the one derived from the discrete model in Figure 8. However, the two remaining hinges at the supports, appear lower (towards the ground), comparing to the discrete models shown in Figure 8.

When an inward settlement of the outer supports by 100 mm is applied on the continuum smeared cracking model, analysis terminates early due to convergence issues and no plastic strain arises. On the contrary, the simulation with the concrete damage plasticity model proceeds and allows the representation of a three-hinge mechanism, as shown in Figure 15. It is noted that the discrete approach presented in the previous section resulted in sliding failure mode at the supports.

For an out of plane settlement of the two internal supports of the bridge, tensile failure takes place at the outer arches, as shown in Figure 16 for the continuum damage plasticity model. This is attributed to the out of plane bending response of the structure. Failure in this case is mainly developed at the top of these arches as well as at the supports. A similar failure mode is obtained from the discrete model shown in Figure 10. For the same load

523 case, a limited compressive failure also appears in the opposite face of the structure, as
524 shown in Figure 17.
525 When an out of plane settlement of 20 mm on the two internal supports of the bridge is
526 combined with a vertical load of 100 kN applied at the one quarter of the span of the middle
527 arch, plastic strain is experienced on the outer side of the middle supports. It is noted that
528 a similar failure behaviour was obtained in Figure 16 for the case out of plane settlement
529 of the inner supports (without vertical point load), indicating that the out of plane
530 movement is the critical loading.
531 For a downward settlement of the two internal supports, the plastic strain distribution
532 shown in Figure 18 is obtained from the concrete damage plasticity model. As depicted in
533 the figure, for each outer arch, two hinges are developed, one close to the internal support
534 and another close to the external one. A similar hinge-pattern is also derived in
535 (Drosopoulos et al. 2008). Moreover, the discrete model's response given in Figure 11,
536 results in a similar hinge-mechanism, but the position of the hinge in the proximity of the
537 internal support of the left outer arch, is different comparing to the corresponding hinge
538 shown in Figure 18.
539 For a final load case, a vertical load of 100 kN is applied at about one quarter of the span
540 of the middle span of the bridge, together with a 20 mm downward movement of the two
541 internal supports. Results indicate a similar failure pattern with the one depicted in Figure
542 18 where downward settlement of the middle supports is considered, without any vertical
543 load.
544
545

Influence of the backfill on the structural response

The presence of the soil backfill above the arch, provides a better load distribution through the body of the backfill towards the arch, which is the main structural component. It also increases the compression above the arch. To highlight the influence of the backfill material on the overall response, a new model is developed, where backfill is simulated using three-dimensional finite elements, as shown in Figures 3c and 3d. For the arch, the continuum concrete damage plasticity law has been considered. Goal of this investigation is to discuss the influence of the backfill on the response, by conducting a comparison with the corresponding results when no backfill was considered.

Four load cases have been implemented in this case, namely the horizontal, outward and inward settlement of the outer supports, the out of plane settlement of the middle supports and the vertical downward force.

In Figure 19 the plastic strain distribution for outward settlement of the outer supports is shown. It is clear that a quite significant failure on the backfill is observed, which is attributed to the low-quality material properties which have been assigned to it. However, it is observed that concerning the response of the arch, although some failure is developed, this is limited comparing to the results obtained from the same load case, without the backfill (Figure 14). In particular, in Figure 14 three hinges were developed in the outer arches, one in the crown and two in the supports. According to Figure 19 the hinges close to the internal support of each outer arch are not developed. In addition, in the left arch, the top hinge is not exactly developed in the middle of the span, but towards the left side. Both comments indicate a change in the hinge-mechanism of the arch, comparing to the analysis without the fill.

For the case of inward settlement of the two outer supports, Figure 20 indicates that three hinges arise in the arch. Their position is the same with the position of the hinges in the model without the backfill (Figure 15), however their distribution in the arch is limited, comparing to Figure 15.

The load case with the out of plane settlement of the two inner supports results in a similar plastic strain distribution in the body of the arch, with the one received from the model without the backfill (Figures 16, 17).

For the last load case, where a vertical downward force is applied on the backfill, in a position near the quarter of the middle span, the plastic strain distribution shown in Figure 21 arises. According to this figure, failure on the arch is mainly developed near the point of the load application. On the contrary, when the backfill was not considered (Figure 13), failure on the arch was developed in four points, resembling the traditional, four-hinge mechanism.

Force - displacement diagrams

Within finite element analysis, force-displacement diagrams can be used to determine the point of failure of a structure. Figure 22 shows the force-displacement diagrams obtained from the different numerical models, which were subject to a vertical load and to a combination of vertical load plus settlement of supports. It can be noticed that the continuum models lead to a more stiff response for (pure) vertical loading, comparing to the discrete models.

In addition, the hinge formation mechanism is the most likely cause of failure compared to material failure in compression, since compressive failure was observed only in one case (limited compressive failure for out of plane settlement of support, Figure 17). The

numerical models with out of plane settlement of supports and with vertical settlement of internal supports combined with a vertical load, are highly unstable. For these load cases, the smeared cracking models resulted in a very low ultimate load, comparing to the discrete models. This is due to the brittle response of the smeared cracking law, when tensile failure arises. On the other hand, the discrete model allows for activation (opening-sliding) of the interfaces, which then lead to redistribution of forces, until a collapse mechanism arises resulting in a higher ultimate load compared to the continuum model.

The concrete damage plasticity models provided the capacity to properly describe the quasi-static response of masonry arches. For the same initial load, which is considered in the previous simulations, this constitutive description leads to a stiff response. For a significantly higher initial load, the force – displacement graph becomes non-linear and the four-hinge mechanism shown in Figure 13 arises.

Conclusions and further recommendations

In this study, the structural behaviour of a masonry arch bridge is investigated, using non-linear finite element models. Various loading cases which can be experienced by the structure have been considered, including settlement of supports. This type of loading may appear due to erosion and heavy water flow. The numerical models used for the structural analysis, were developed based on in-situ survey of the existing geometry. The three-dimensional geometry used for the investigation was obtained on AutoCAD, using a cloud of points of the bridge collected by researchers in Turkey. A terrestrial laser scanner was used to obtain these points. The geometry was then imported in Abaqus, which is a commercial finite element package.

Two modelling approaches were considered, adopting a discrete and a continuum constitutive description. According to the first approach, unilateral frictional contact interfaces were used to simulate the real contact conditions between the stones. Within the second approach, continuum constitutive descriptions were used, relying on a smeared cracking formulation and on a concrete damage plasticity law. The developed models were strongly non-linear due to the presence of the interfaces and of the non-linear material description. The Newton-Raphson incremental – iterative process was used to solve the numerical problem.

From the different finite element models presented in this study, different failure modes of the masonry arch were observed, for the various load cases.

The following conclusions can be drawn from this study:

- The critical failure pattern obtained from the discrete models is the formation of hinge-mechanisms, which can be developed both in-plane and out-of-plane, for corresponding loads. It is observed that the three hinge-mechanism obtained in published research for horizontal, outward and inward settlement of supports of single arch-bridges, also arises from the discrete approach, adopted in this article for multi-span arches. Similarly, when a vertical, downward settlement of support takes place, two hinges are developed in the affected arches. The same conclusion has been derived in old studies, for single-span arches. A four-hinge failure mechanism arises for a vertical load at the middle arch.
- The numerical models which compute the out of plane loads are computationally expensive and highly unstable, hence, the corresponding simulations terminate before the full load is assigned.

- The contribution of the backfill soil material, which is found above the arch, may significantly influence the structural response. It is shown in this study that the presence of backfill may alter the failure pattern in the arch, leading to limited damage.
- The difference in the mechanical response, which is derived from discrete and continuum laws, is highlighted in the article. The discrete approach allows for the formation of hinges and sliding failure modes, resulting in a more flexible approximation of the structural response. On the contrary, the continuum approach leads to more stiff response. In addition, the discrete approach may lead to numerical instabilities and increased computational cost due to the presence of multiple unilateral contact-friction interface.
- The continuum approach results in easy modelling. Tensile plastic strain distribution is the dominant failure pattern depicted by this approach. Numerical instabilities may arise when point forces are considered, due to local failure near the points of the load application. From the two continuum constitutive descriptions, the smeared cracking law results in convergence difficulties, attributed to the brittle nature of this description. The concrete damage plasticity law, making use of damage variables, better describes the quasi-brittle response of the masonry arch. The failure patterns which are obtained from the continuum concrete damage plasticity law, are similar to the ones derived from the discrete approach and the results found in published research.

Future research may include the investigation of the influence of the spandrel walls on the mechanical response of masonry arch bridges. Finally, the incorporation of other advanced

numerical tools in the study of arches, such as the cohesive zone modelling approach, is also left for future investigation.

Acknowledgements

The authors thank the General Directorate of Highways of Turkey, for providing access to the data of the presented monument.

Data Availability Statement

All data, models, and code generated or used during the study appear in the submitted article.

References

Armesto, J., Roca-Pardiñas, J., Lorenzo, H., and Arias, P. (2010). "Modelling masonry arches shape using terrestrial laser scanning data and nonparametric methods." *Engineering Structures*, 32(2), 607-615.

Ashurst, D. (1992). "An assessment of repair and strengthening techniques for brick and stone masonry arch bridges."

Ataei, S., Jahangiri Alikamar, M., and Kazemiashtiani, V. (2016). "Evaluation of axle load increasing on a monumental masonry arch bridge based on field load testing." *Construction and Building Materials*, 116, 413-421.

Belarbi, A., and Hsu, T. T. (1994). "Constitutive laws of concrete in tension and reinforcing bars stiffened by concrete." *Structural Journal*, 91(4), 465-474.

Campbell, J. W., and Tutton, M. (2013). *Staircases: History, repair and conservation*, Routledge.

Casapulla, C., Mousavian, E., and Zarghani, M. (2019). "A digital tool to design structurally feasible semi-circular masonry arches composed of interlocking blocks." *Computers & Structures*, 221, 111-126.

Catalan, R., and Aldea, L. "New tendencies on repair and strengthening on masonry arch bridges." *Proc., 5th International Conference on Arch Bridges*, 12-14.

CEN (2005). "Eurocode 6: Design of masonry structures. Part 1-1: General rules for reinforced and unreinforced masonry structures."

Conde, B., Ramos, L. F., Oliveira, D. V., Riveiro, B., and Solla, M. (2017). "Structural assessment of masonry arch bridges by combination of non-destructive testing

techniques and three-dimensional numerical modelling: Application to Vilanova bridge." *Engineering Structures*, 148, 621-638.

Crisfield, M. (1985). "FINITE ELEMENT AND MECHANISM METHODS FOR THE ANALYSIS OF MASONRY AND BRICKWORK ARCHES. RESEARCH REPORT."

Domede, N., Sellier, A., and Stablon, T. (2013). "Structural analysis of a multi-span railway masonry bridge combining in situ observations, laboratory tests and damage modelling." *Engineering Structures*, 56, 837-849.

Drosopoulos, G. A., Stavroulakis, G. E., and Massalas, C. V. (2008). "Influence of the geometry and the abutments movement on the collapse of stone arch bridges." *Construction and Building Materials*, 22(3), 200-210.

Erdoğan, Y. (2011). "Engineering properties of Turkish travertines." *Scientific Research and Essays*, 6(21), 4551-4566.

Ford, T., Augarde, C., and Tuxford, S. "Modelling masonry arch bridges using commercial finite element software." *Proc., the 9th International Conference on Civil and Structural Engineering Computing, Netherlands*, 161-203.

GDH (2017). "Burdur province, Bucak district, Dağarcık bridge technical report." *General Directorate of Highways, 13th Region*Antalya, Turkey (In Turkish).

Gönen, S., and Soyöz, S. (2021). "Seismic analysis of a masonry arch bridge using multiple methodologies." *Engineering Structures*, 226, 111354.

Guastavino, R., and Moreno, R. G. (2006). *Escritos sobre la construcción cohesiva y su función en la arquitectura*, Reverte.

Heyman, J. (1982). *The Mansonry Arch*, Ellis Horwood Limted, England.

715 Hibbitt, D., Karlsson, B., and Sorensen, P. (2012). "Abaqus 6.12. 3 Manual." *Dassault*
716 *Systèmes Simulia Corp., Providence, RI*.
717 Hognestad, E. (1951). "Study of combined bending and axial load in reinforced concrete
718 members." University of Illinois at Urbana Champaign, College of Engineering ….
719 Hughes, T., Blackler, M., and MEXE (1997). "A review of the UK masonry arch
720 assessment methods." *Proceedings of the Institution of Civil Engineers-Structures*
721 *and Buildings*, 122(3), 305-315.
722 Hughes, T. G., Hee, S., and Soms, E. (2002). "Mechanism analysis of single span masonry
723 arch bridges using a spreadsheet." *Proceedings of the Institution of Civil Engineers-*
724 *Structures and Buildings*, 152(4), 341-350.
725 Lubliner, J., Oliver, J., Oller, S., and Onate, E. (1989). "A plastic-damage model for
726 concrete." *International Journal of solids and structures*, 25(3), 299-326.
727 Lubowiecka, I., Armesto, J., Arias, P., and Lorenzo, H. (2009). "Historic bridge modelling
728 using laser scanning, ground penetrating radar and finite element methods in the
729 context of structural dynamics." *Engineering Structures*, 31(11), 2667-2676.
730 Maravelakis, E., Konstantaras, A., Kritsotaki, A., Angelakis, D., and Xinogalos, M. (2013).
731 "Analysing User Needs for a Unified 3D Metadata Recording and Exploitation of
732 Cultural Heritage Monuments System." Springer Berlin Heidelberg, 138-147.
733 Melbourne, C. (1991). "Conservation of masonry arches in Proc 9 th Intern." *Brick/Block*
734 *Masonry Conference*Berlin: Deutsche Gesellschaft für Maurerwerksbau e.V.,
735 1563-1570.
736 Melbourne, C., and Gilbert, M. (1995). "The behaviour of multiring brickwork arch
737 bridges." *Structural Engineer*, 73(3).

738 Melbourne, C., McKibbins, L., Sawar, N., and Sicilia Gaillard, C. (2006). "Masonry arch
739 bridges: condition appraisal and remedial treatment." *CIRIA, London*.
740 Motsa, S. M., Drosopoulos, G. A., Stavroulaki, M. E., Maravelakis, E., Borg, R. P., Galea,
741 P., d'Amico, S., and Stavroulakis, G. E. (2020). "Structural investigation of
742 Mnajdra megalithic monument in Malta." *Journal of Cultural Heritage*, 41, 96-105.
743 Mousavian, E., and Casapulla, C. (2020). "Quantifiable feasibility check of masonry
744 assemblages composed of interlocking blocks." *Advances in Engineering Software*,
745 149, 102898.
746 Page, J. (1993). *Masonry arch bridges - Transport Research Laboratory*, London : HMSO.
747 Pulatsu, B., Erdogmus, E., and Lourenço, P. B. (2019). "Comparison of in-plane and out-
748 of-plane failure modes of masonry arch bridges using discontinuum analysis."
749 *Engineering Structures*, 178, 24-36.
750 RING (2021). "LimitState:RING - Powerful masonry arch analysis software."
751 <https://www.limitstate.com/ring>.
752 Sarhosis, V., De Santis, S., and de Felice, G. (2016). "A review of experimental
753 investigations and assessment methods for masonry arch bridges." *Structure and*
754 *Infrastructure Engineering*, 12(11), 1439-1464.
755 Sevim, B., Bayraktar, A., Altunişik, A., Atamturktur, S., and Birinci, F. (2011).
756 "Assessment of nonlinear seismic performance of a restored historical arch bridge
757 using ambient vibrations." *Nonlinear Dynamics*, 63, 755-770.
758 Towler, K. "Applications of non-linear finite element codes to masonry arches." *Proc.*,
759 *Civil-Comp 85, Proceedings*.

760 Van Beek, G. W. (1987). "Arches and vaults in the ancient Near East." *Scientific American*,
761 257(1), 96-103.
762 Wilmers, W. (2012). "Restoration of masonry arch bridges." *Proceedings of the ICE -*
763 *Bridge Engineering*, 165, 135-146.
764 Zampieri, P., Tecchio, G., Da Porto, F., and Modena, C. (2015). "Limit analysis of
765 transverse seismic capacity of multi-span masonry arch bridges." *Bulletin of*
766 *Earthquake Engineering*, 13(5), 1557-1579.

767
768
769
770
771
772
773
774
775
776
777
778
779
780
781

Tables

Table 1: List of models developed.

Model No.	Model Description
Model 1	Pure discrete
Model 2	Continuum with concrete smeared cracking law
Model 3	Continuum with concrete damage plasticity law
Model 4	Discrete with concrete smeared cracking law
Model 5	Discrete with concrete damage plasticity law
Model 6	Continuum model for the arch and the fill, adopting the Mohr-Coulomb failure criterion for the fill and the concrete damage plasticity law for the arch

Table 2: Concrete smeared cracking law parameters for the stones used in the arch bridge.

Concrete Smeared Model			
Yield Stress (MPa)	Compressive stress (MPa)	Ratio of uniaxial tension to compression failure stress	Ratio of biaxial to uniaxial compression failure stress
28	70	0.1	1.16

Table 3: Concrete Damage Plasticity model parameters for the stones used in the arch bridge.

Concrete Damage Plasticity Model				
Dilation Angle	Flow potential eccentricity	Ratio of biaxial to uniaxial compression failure stress	Ratio of second stress invariant of the tensile meridian to the compression meridian	Viscosity Parameter
35	0.1	1.16	0.67	0
Compression behaviour				
Yield Stress (MPa)	Compressive strength (MPa)	ε^{c}_{0} (Strain at maximum compressive strength)	ε^{c}cu (Maximum strain)	ε^{c}pl (Final plastic strain)
28	70	0.00887199	0.01774398	0.00177440
Tension behaviour				
Yield Stress (MPa)	ε^{t}cr (Strain at the tensile yield stress)		ε^{t}pl (Final plastic strain)	
7	0.00044360		0.00443599	

Table 4: Mechanical properties for the stones used in the arch bridge (GDH 2017) .

Material	Young's modulus, E (GPa)	Density (kg/m^3)	Poisson's ratio
Travertine	15.780	2300	0.3

805 *Table 5: Mechanical properties for fill used in the arch bridge (GDH 2017).*

Young's modulus, E (GPa)	Poisson's ratio	Density (kg/m^3)	Angle of internal friction (degrees)	Cohesion (KPa)	Dilation angle (degrees)
0.3	0.3	2000	37	10	24

806

807

808 *Table 6: List of load cases considered in the study.*

Load Case No.	**Load case description**
(a)	Vertical load applied at about one quarter of the middle span of the bridge.
(b)	Horizontal, outward displacement of 100 mm in the plane of the bridge, on both outer supports.
(c)	Horizontal inward displacement of 100 mm in the plane of the bridge on both outer supports.
(d)	100 mm horizontal displacement of the two internal supports in the direction of the water flow, perpendicular to the plane of the bridge.
(e)	Vertical load applied at about one quarter span of the middle span of the bridge with 20 mm displacement of the two internal supports in the direction of the water flow perpendicular to the plane of the bridge
(f)	100 mm downward displacement of the two internal supports.
(g)	Vertical load applied at about one quarter span of the middle span of the bridge with 20 mm downward displacement of the two internal supports.
(h)	Incorporation of backfill - Horizontal, outward displacement of 100 mm in the plane of the bridge, on both outer supports.
(i)	Incorporation of backfill - Horizontal inward displacement of 100 mm in the plane of the bridge on both outer supports.
(j)	Incorporation of backfill - 100 mm horizontal displacement of the two internal supports in the direction of the water flow, perpendicular to the plane of the bridge.
(k)	Incorporation of backfill - Vertical load applied at about one quarter of the middle span of the bridge.

809

810

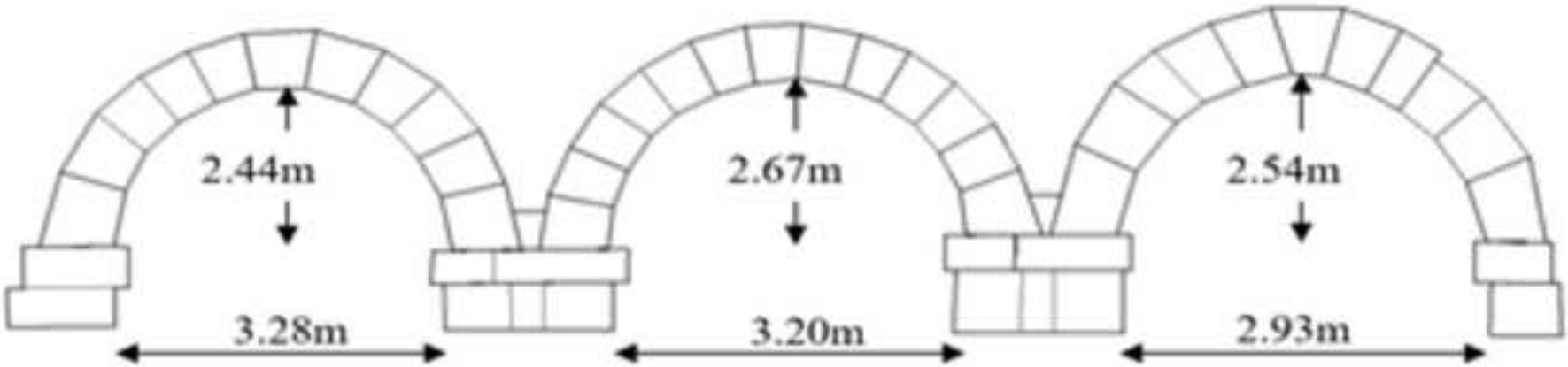

Figure

Click here to access/download;Figure;2c.tif

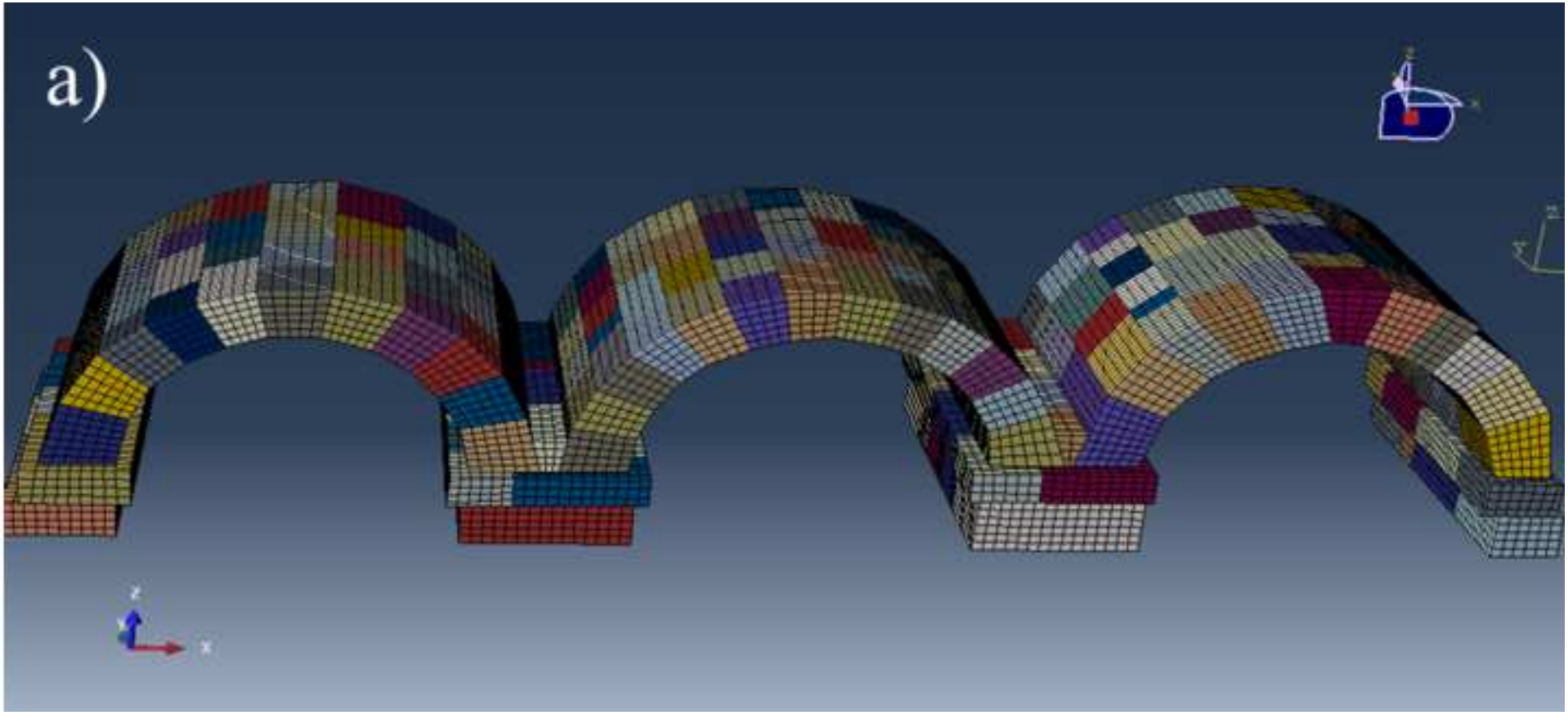

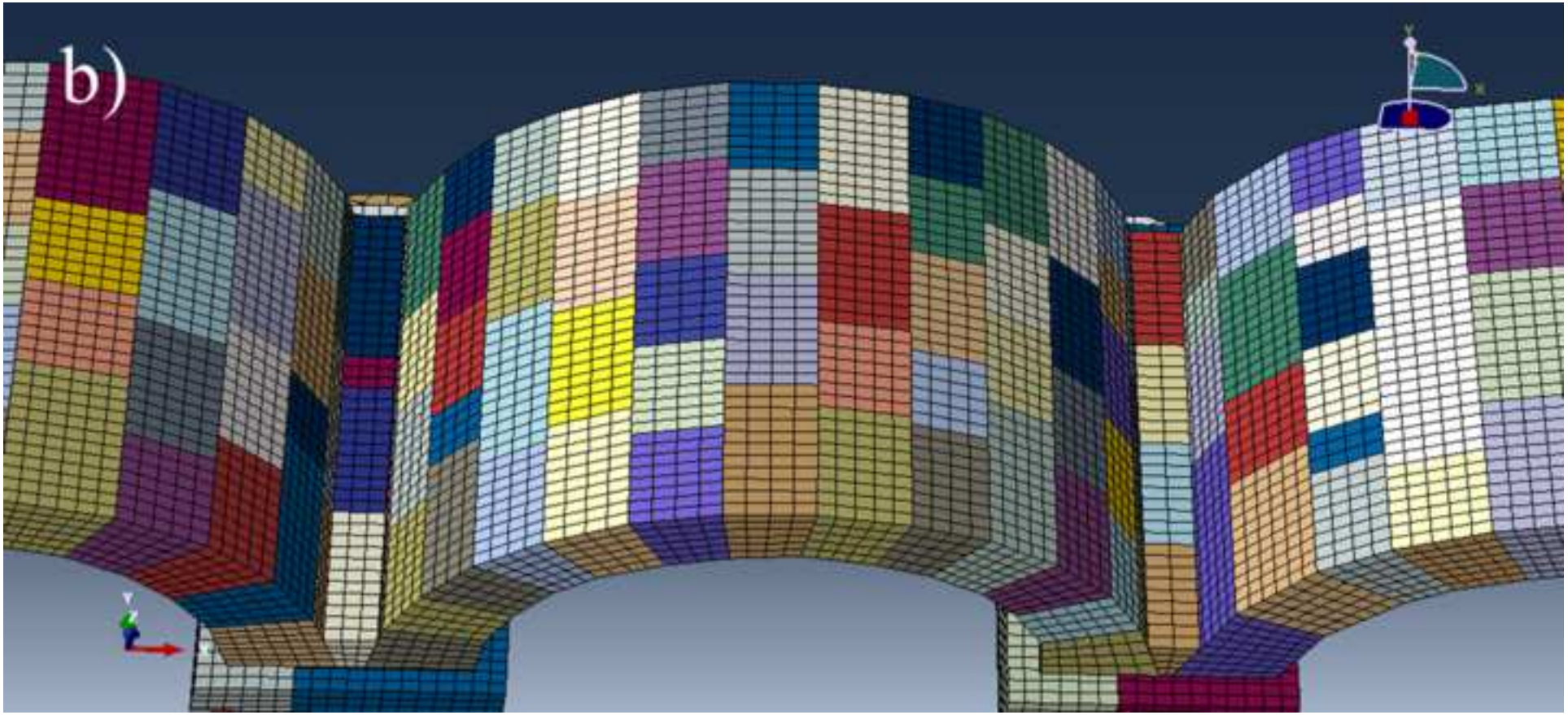

c)

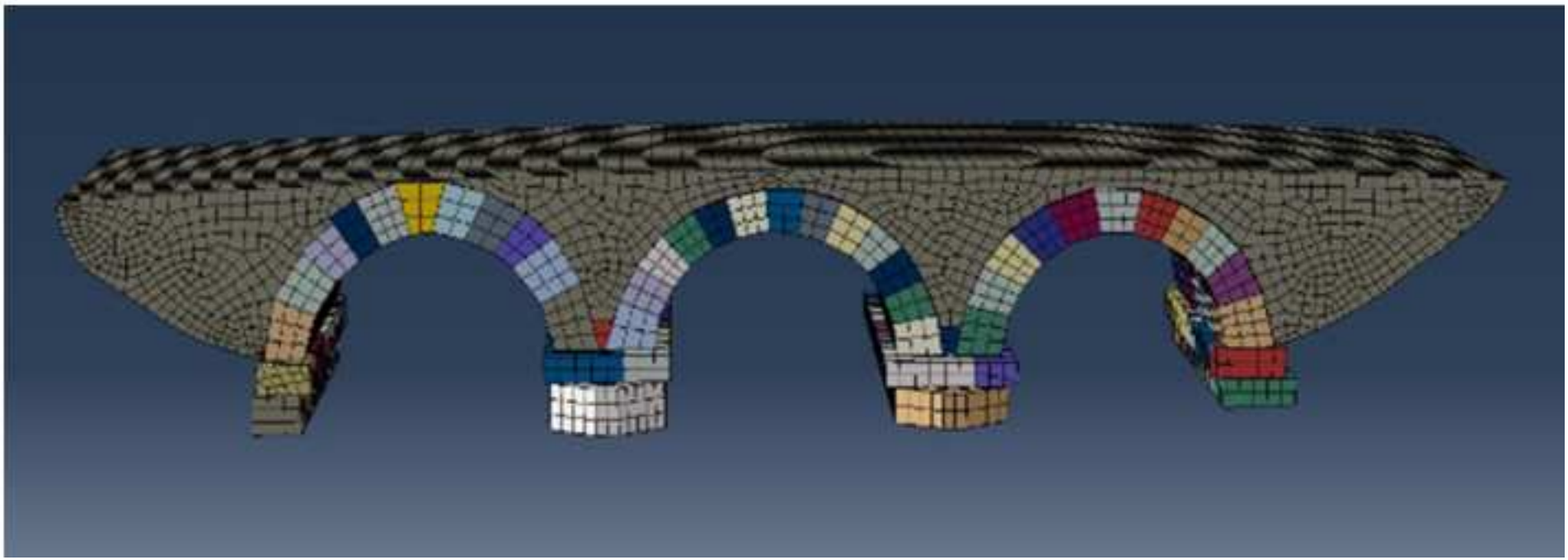

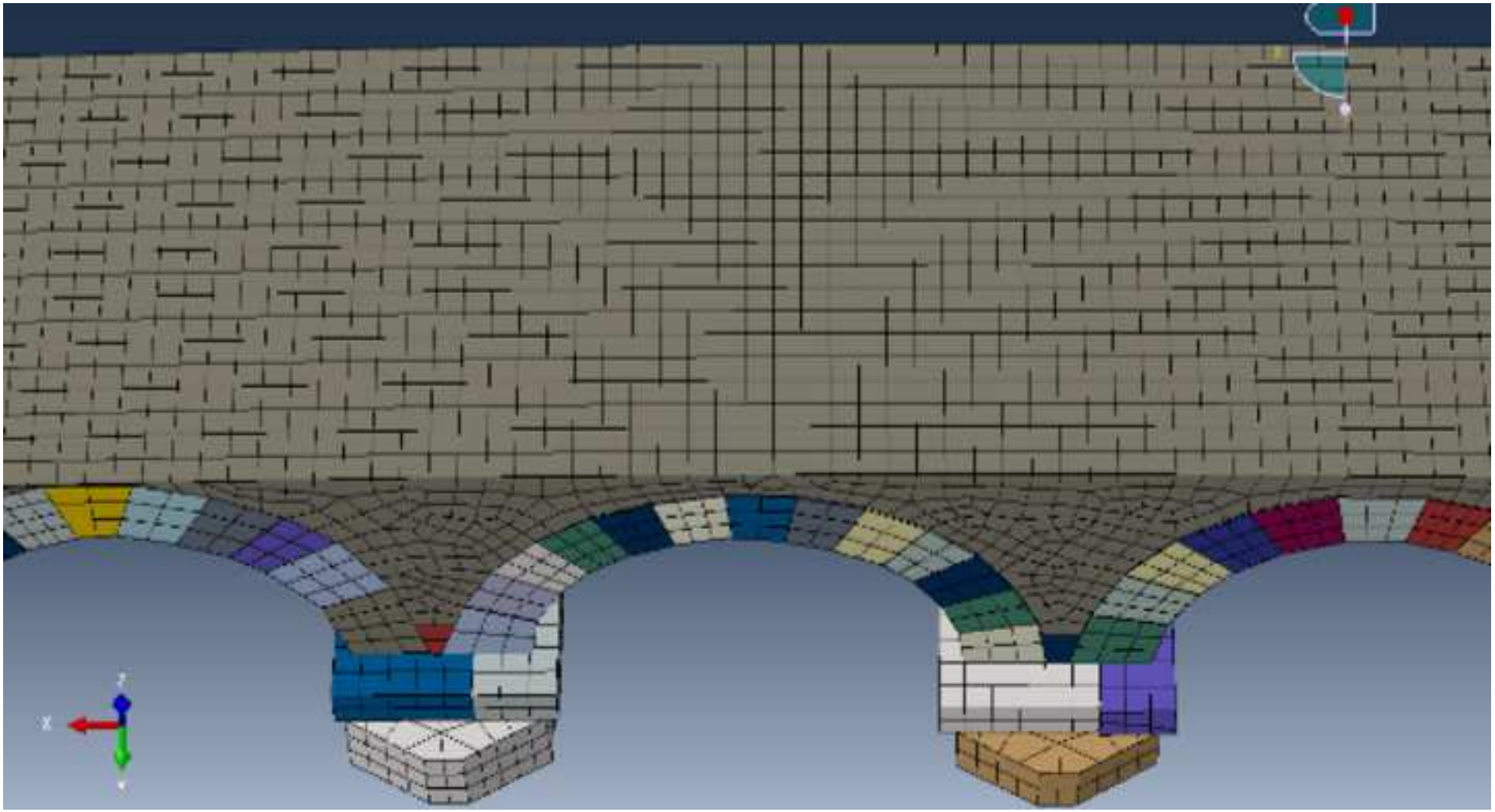

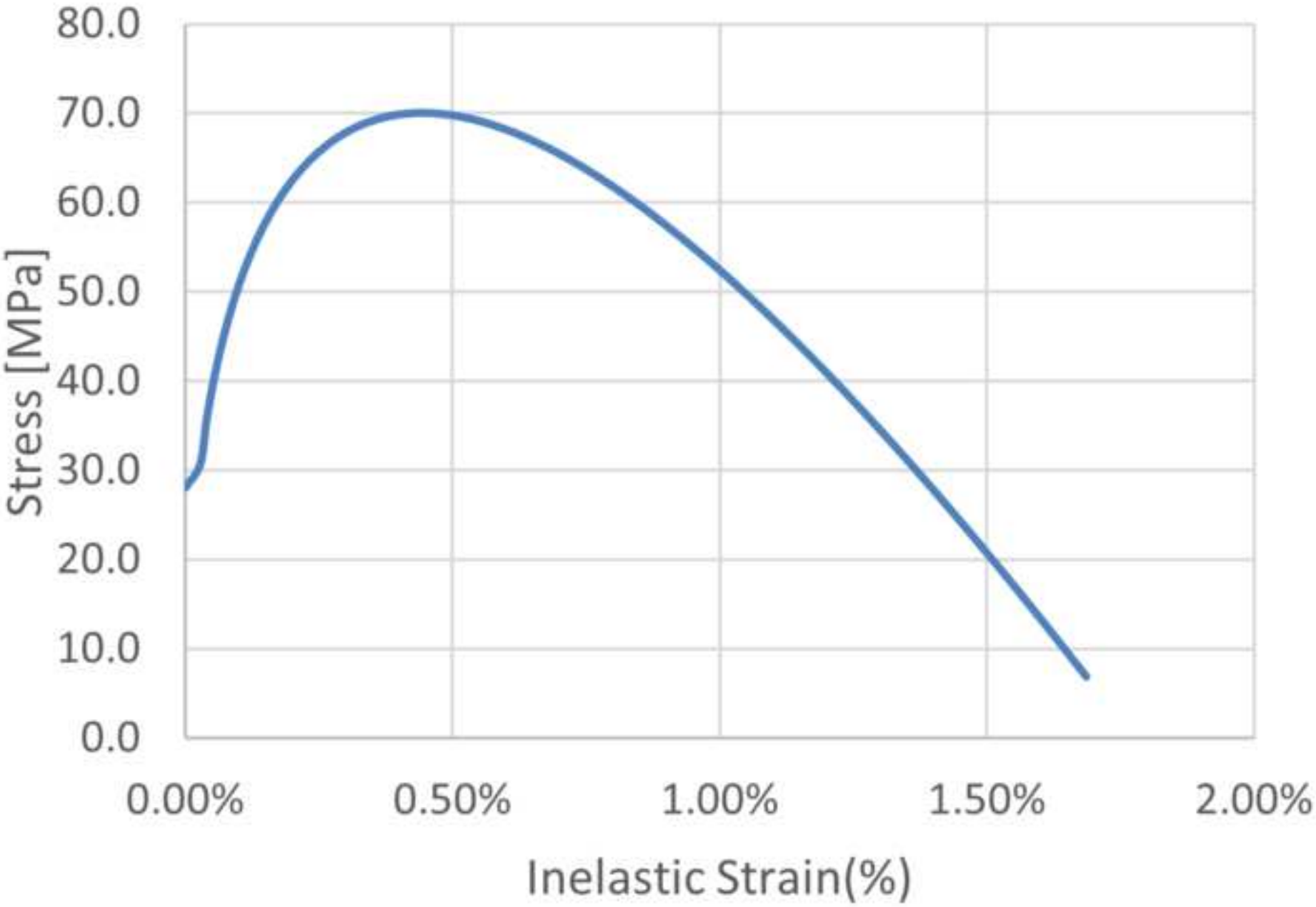

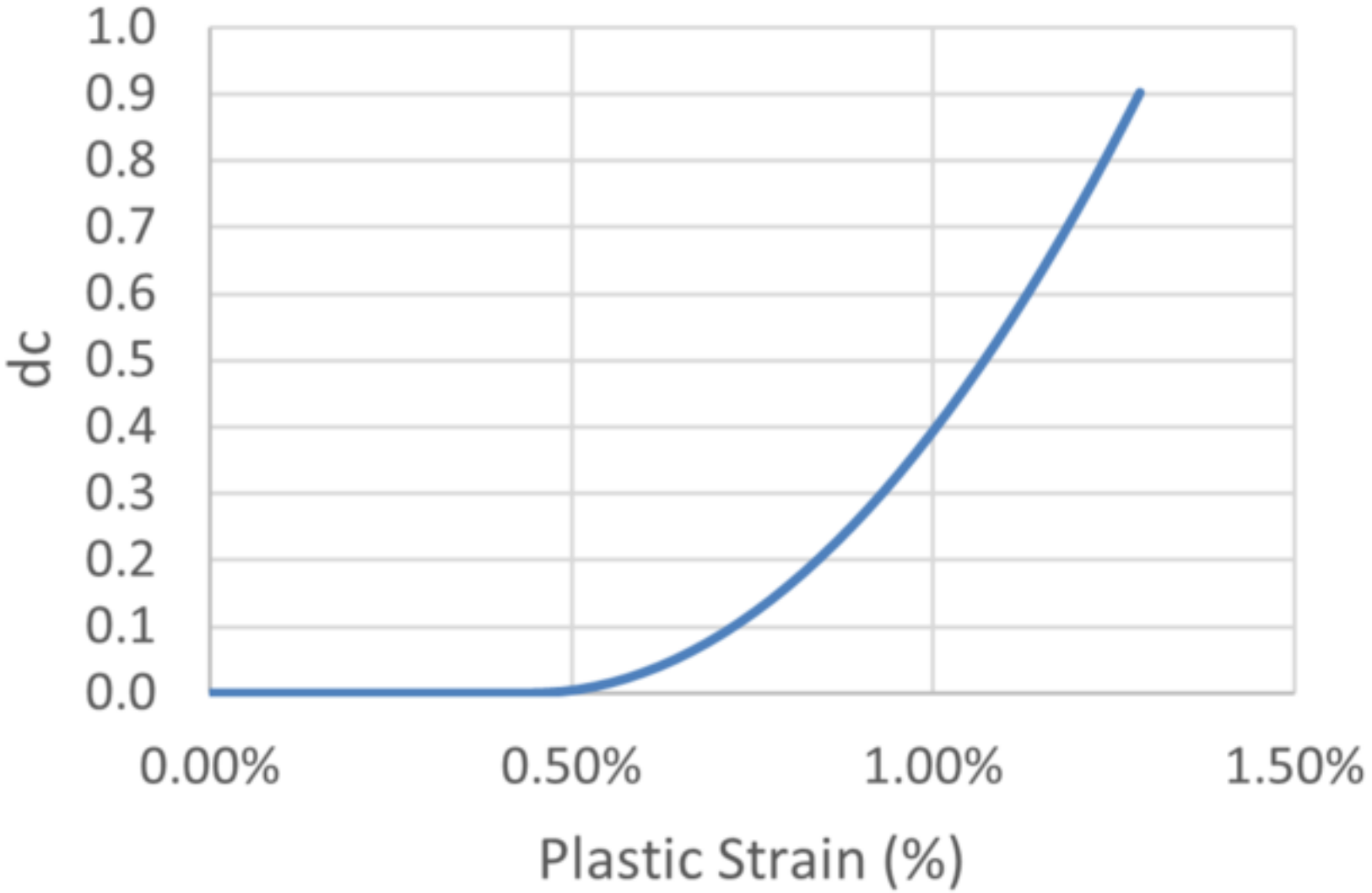

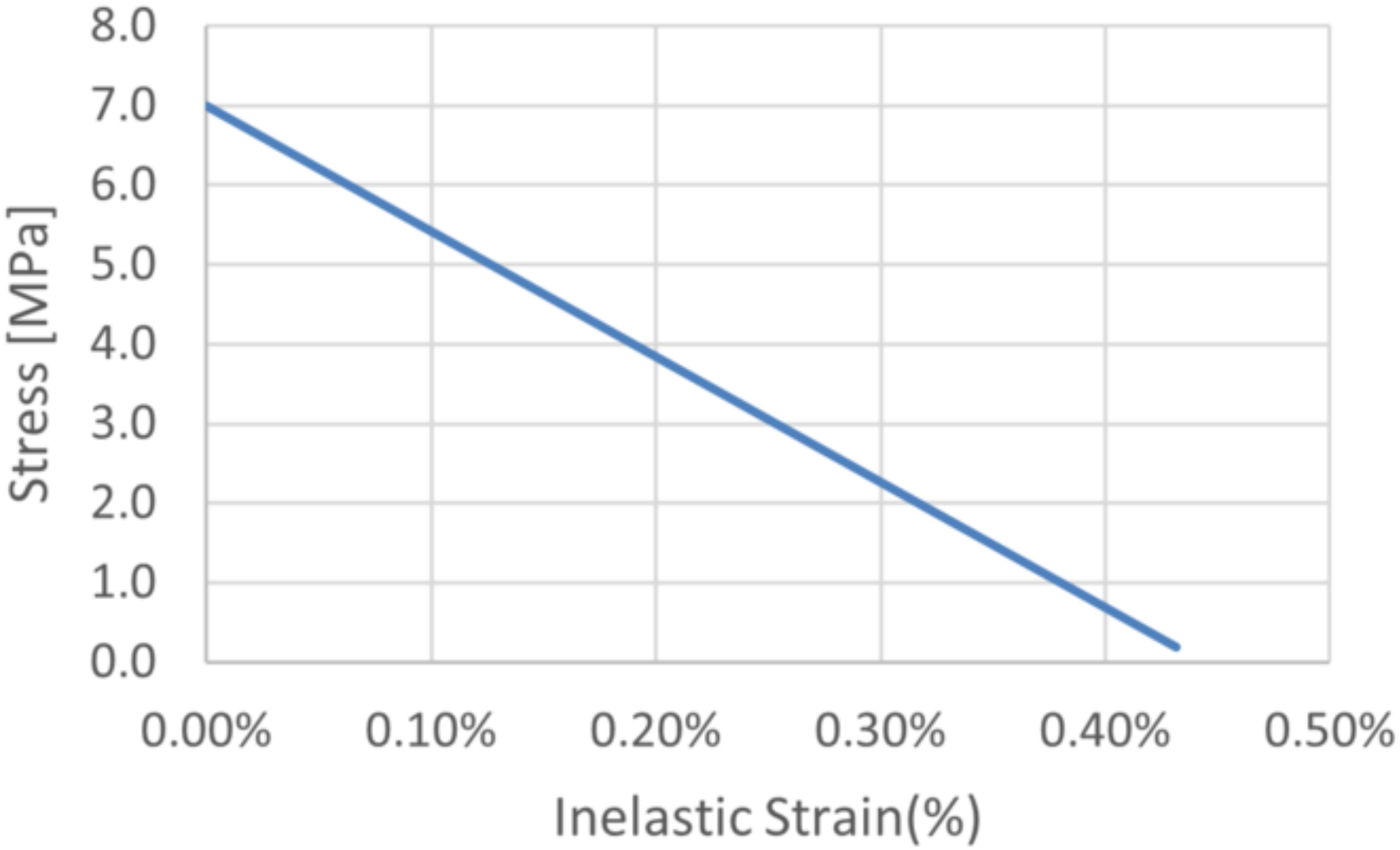

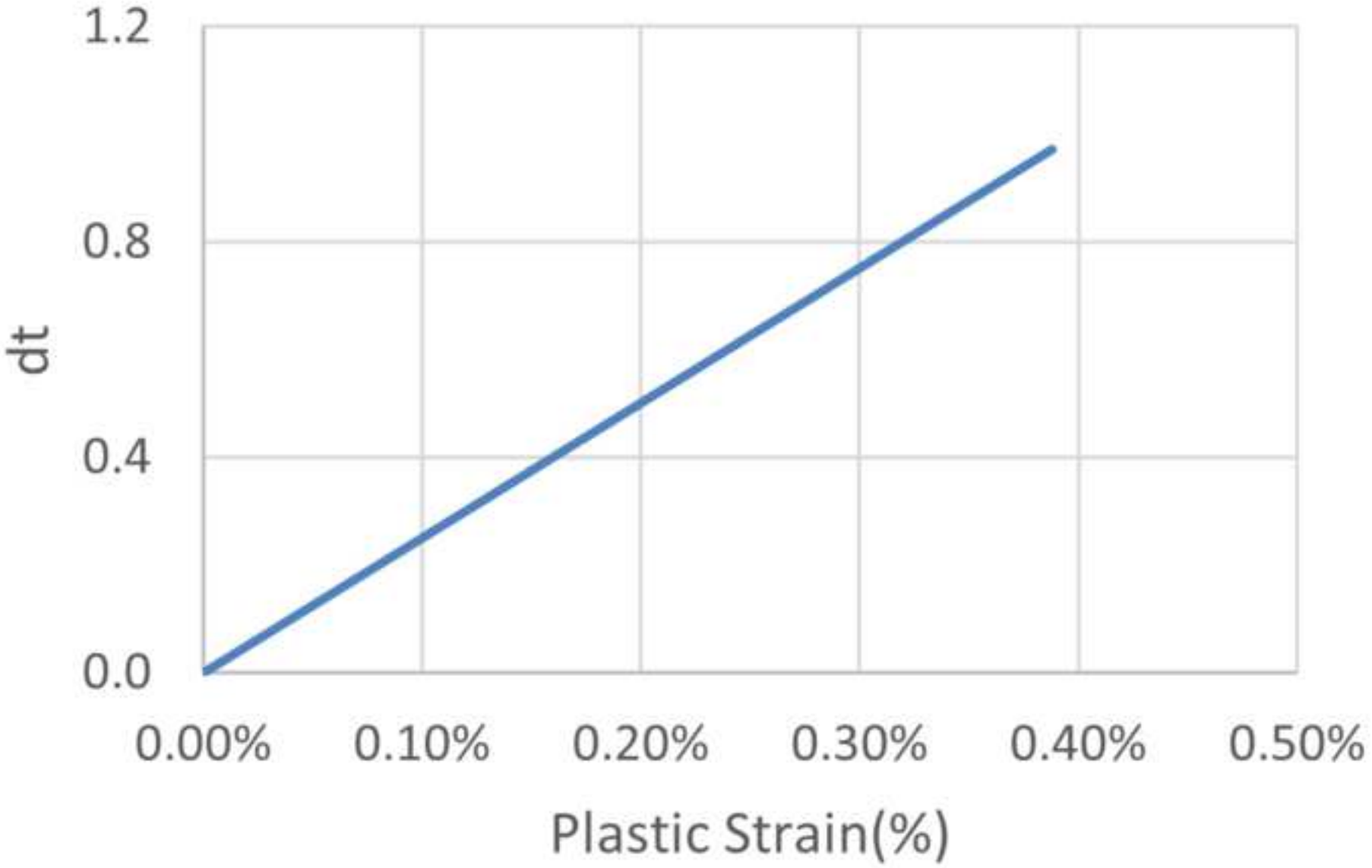

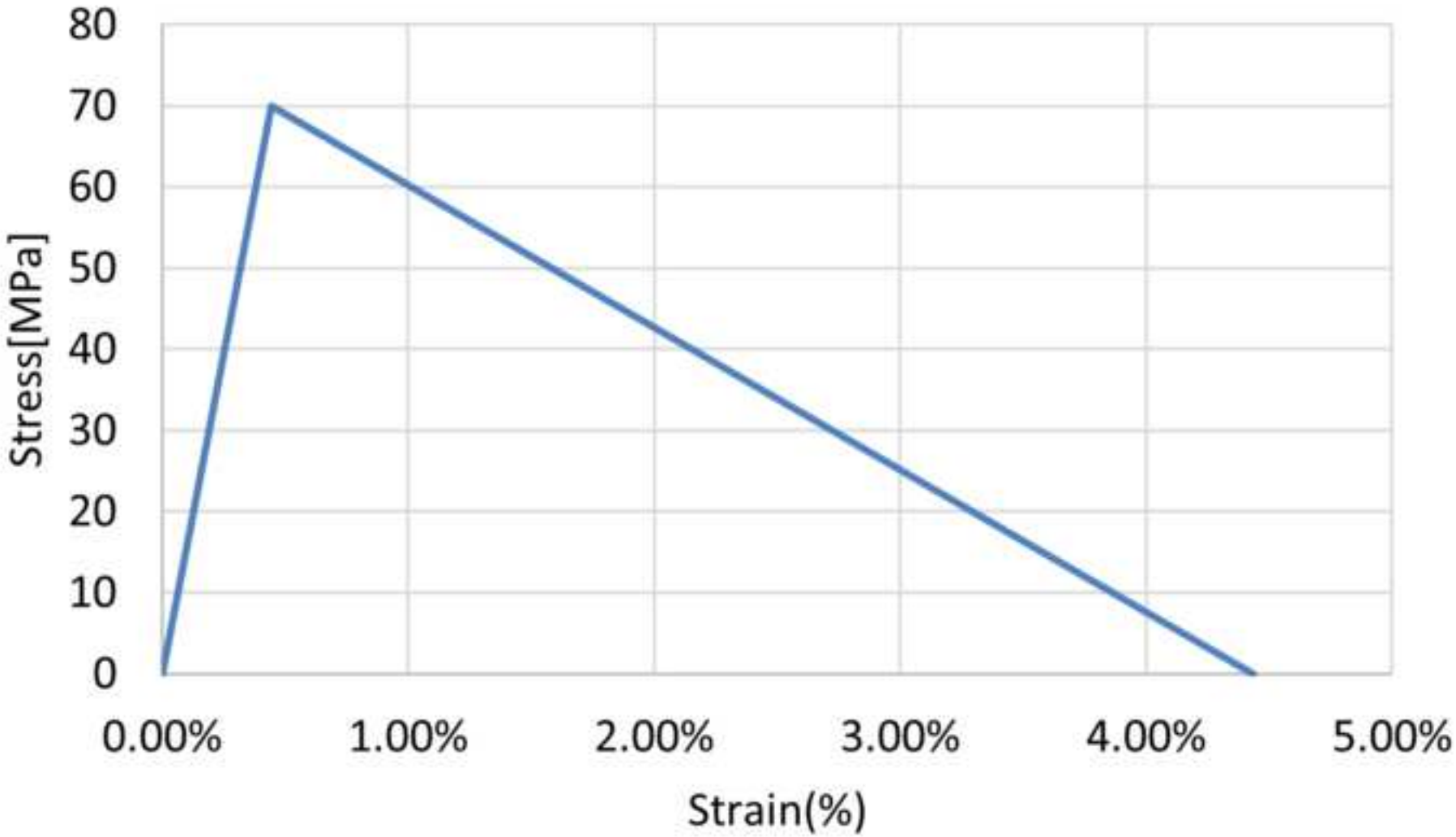

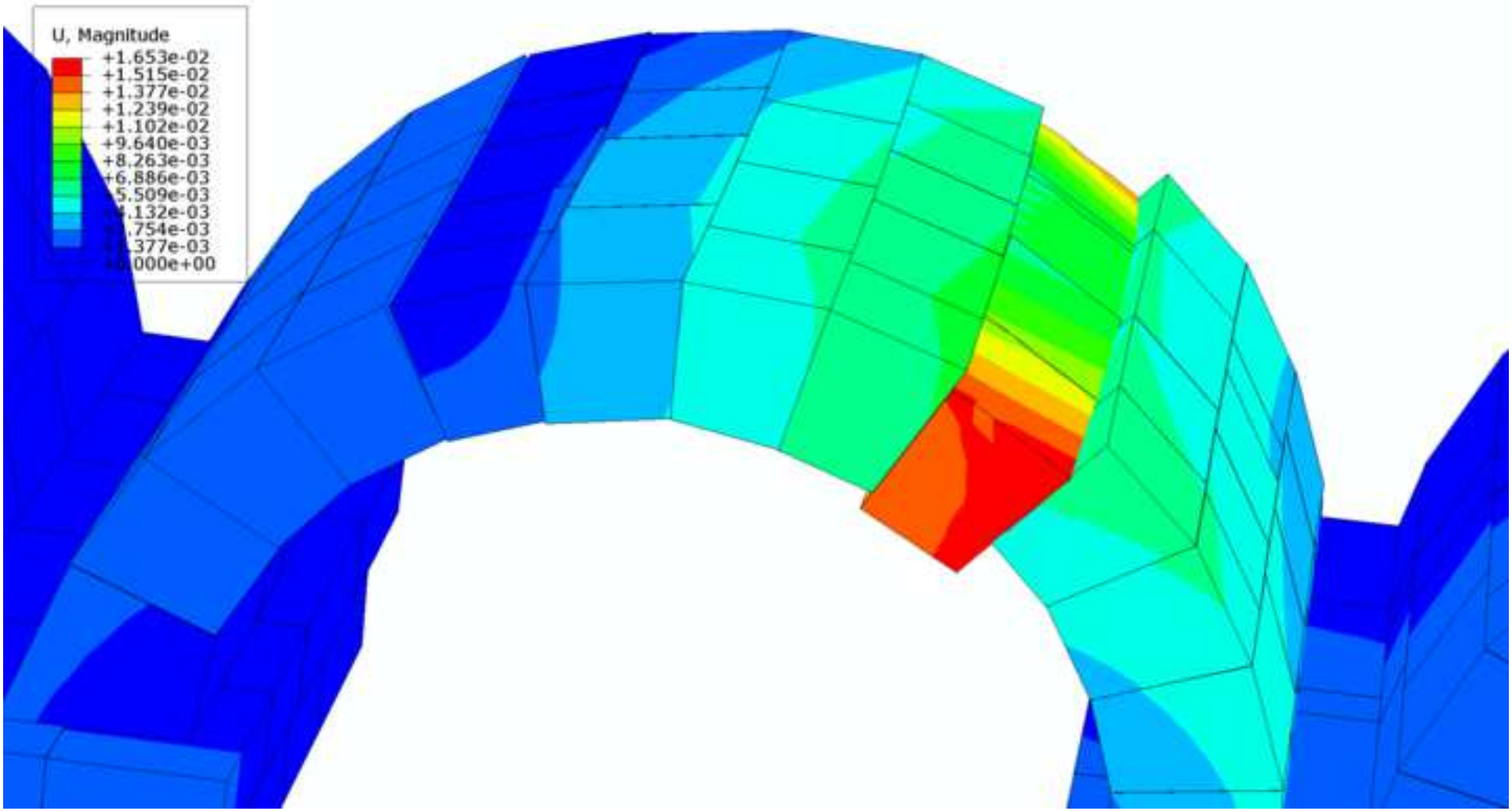

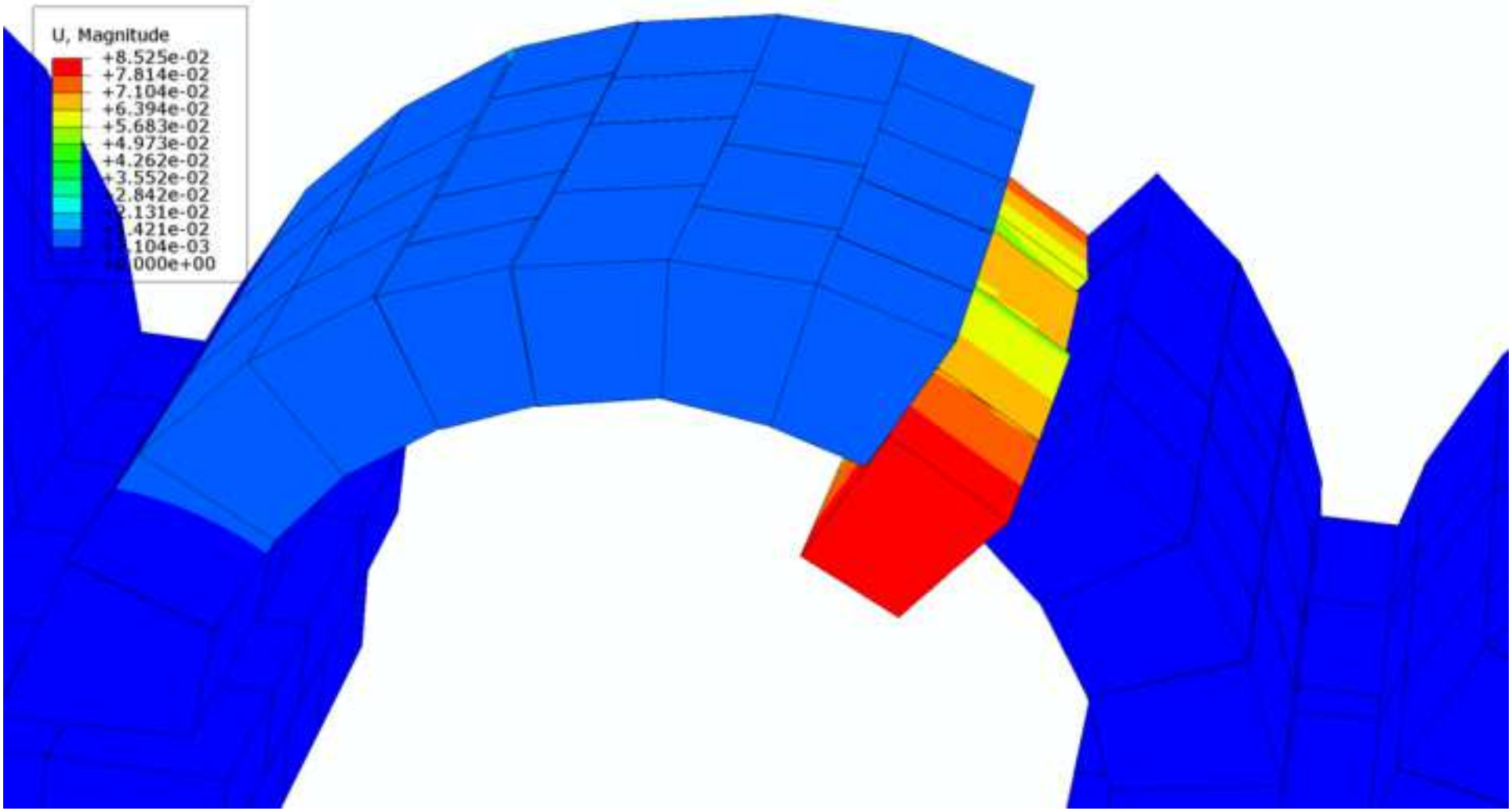

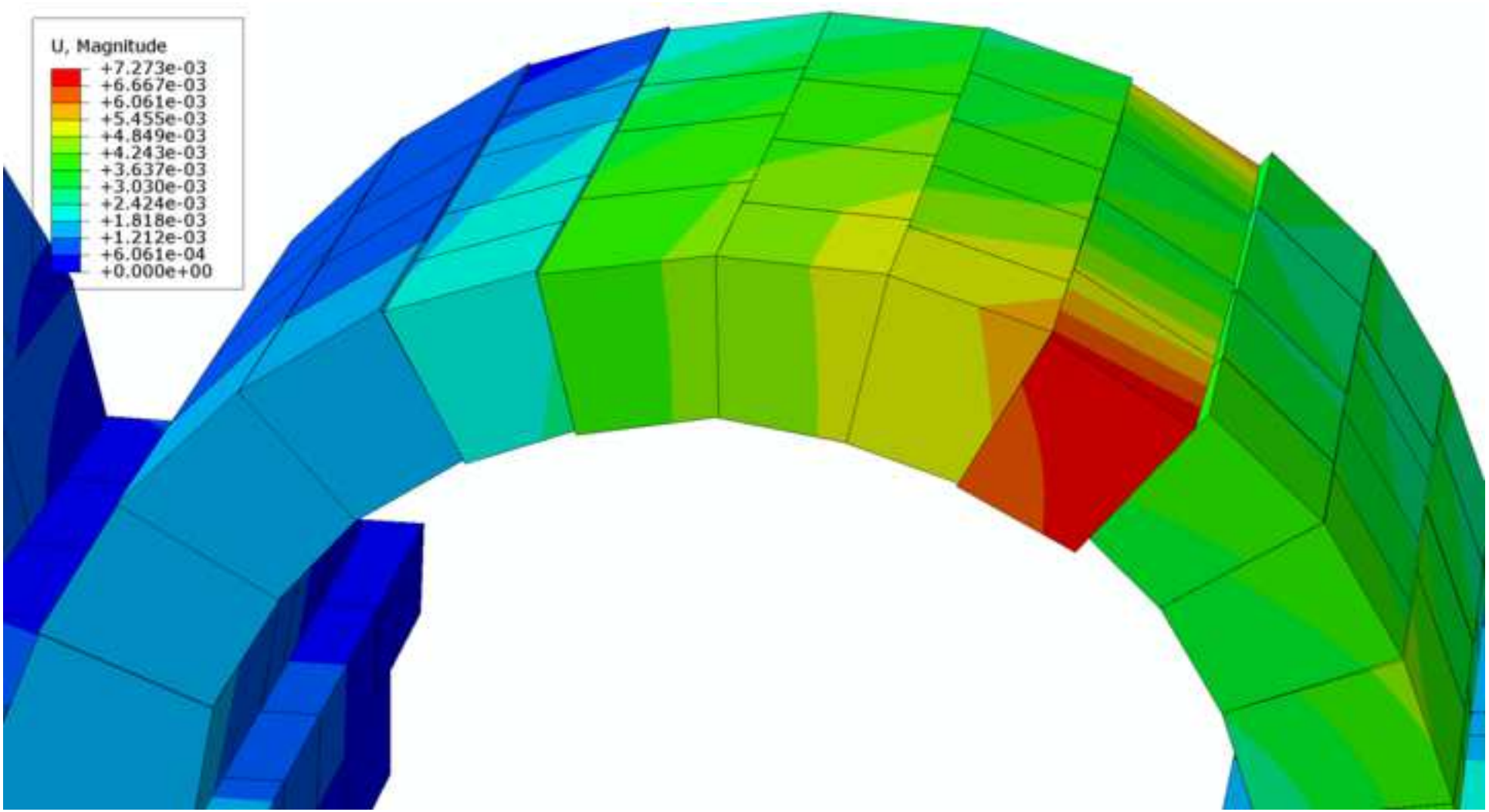

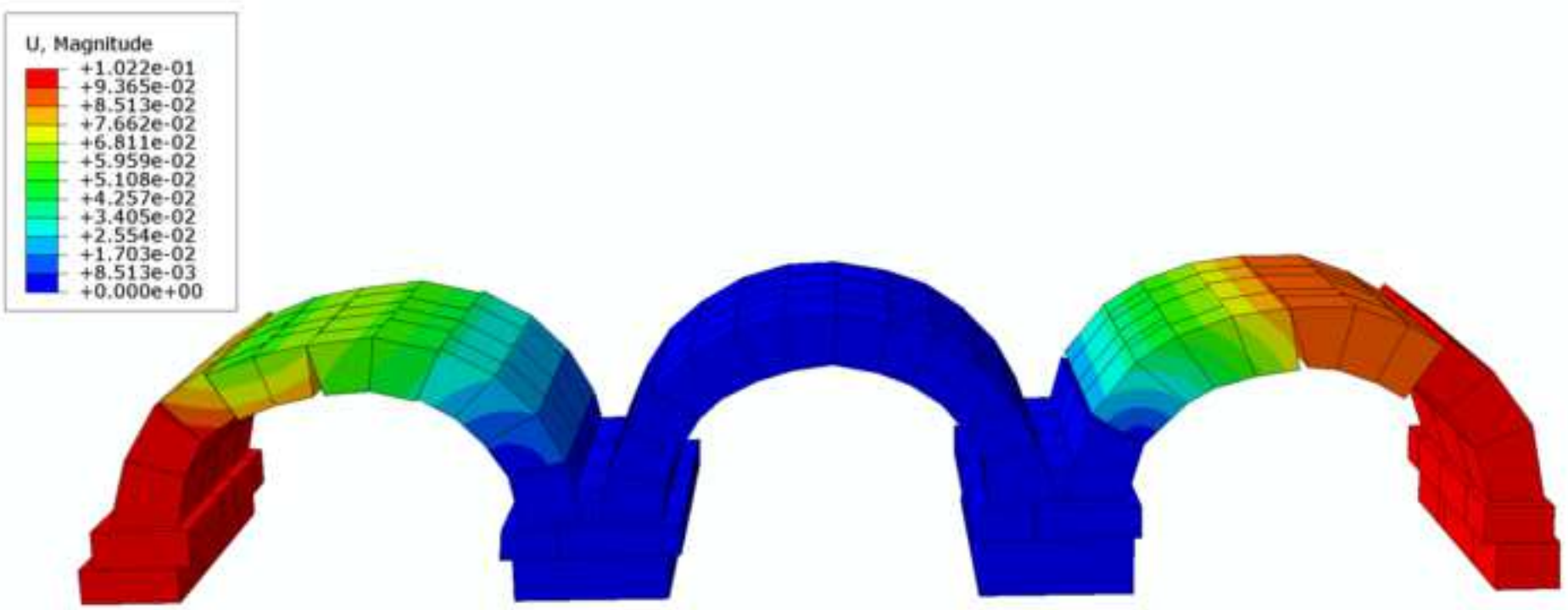

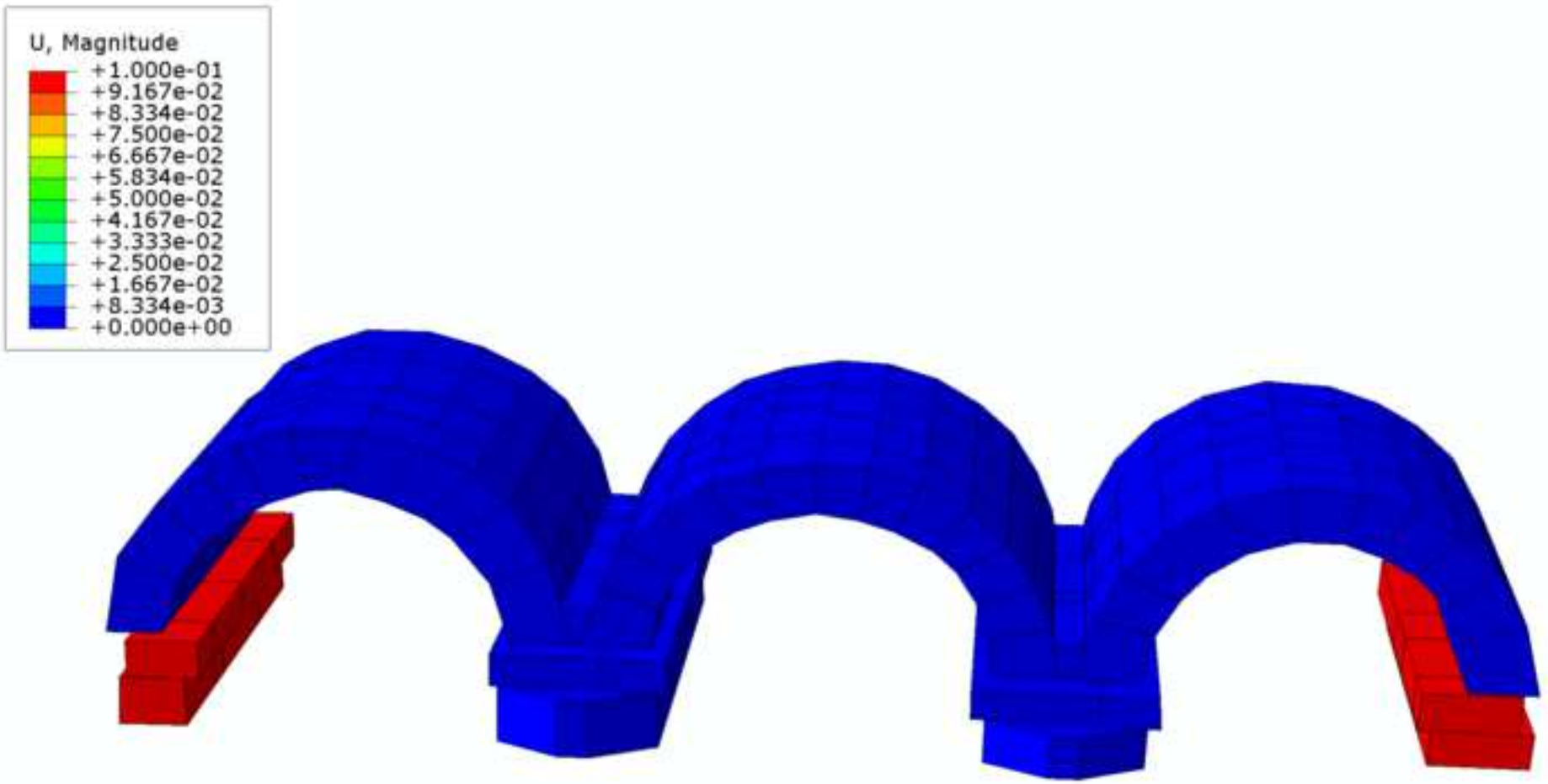

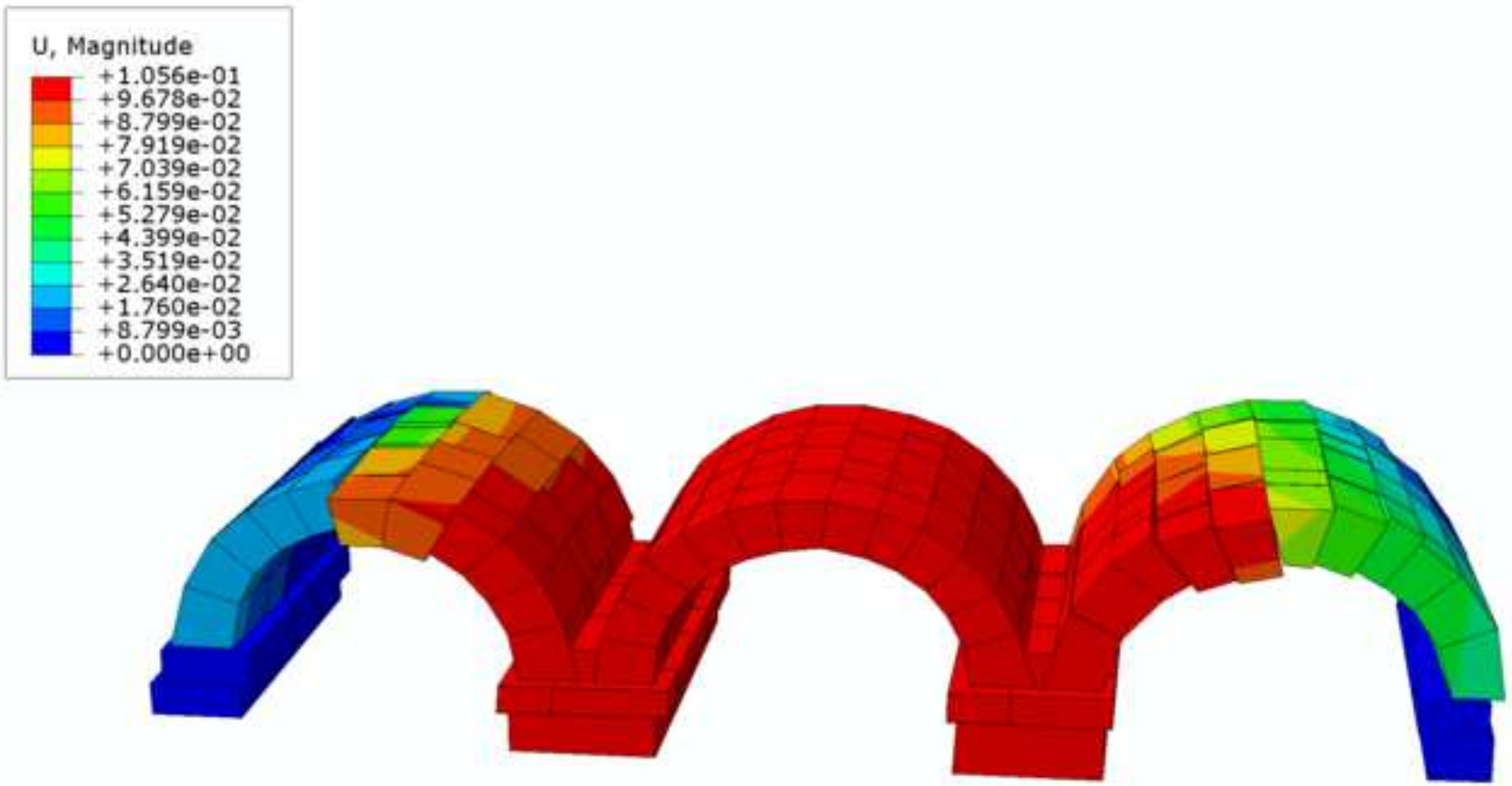

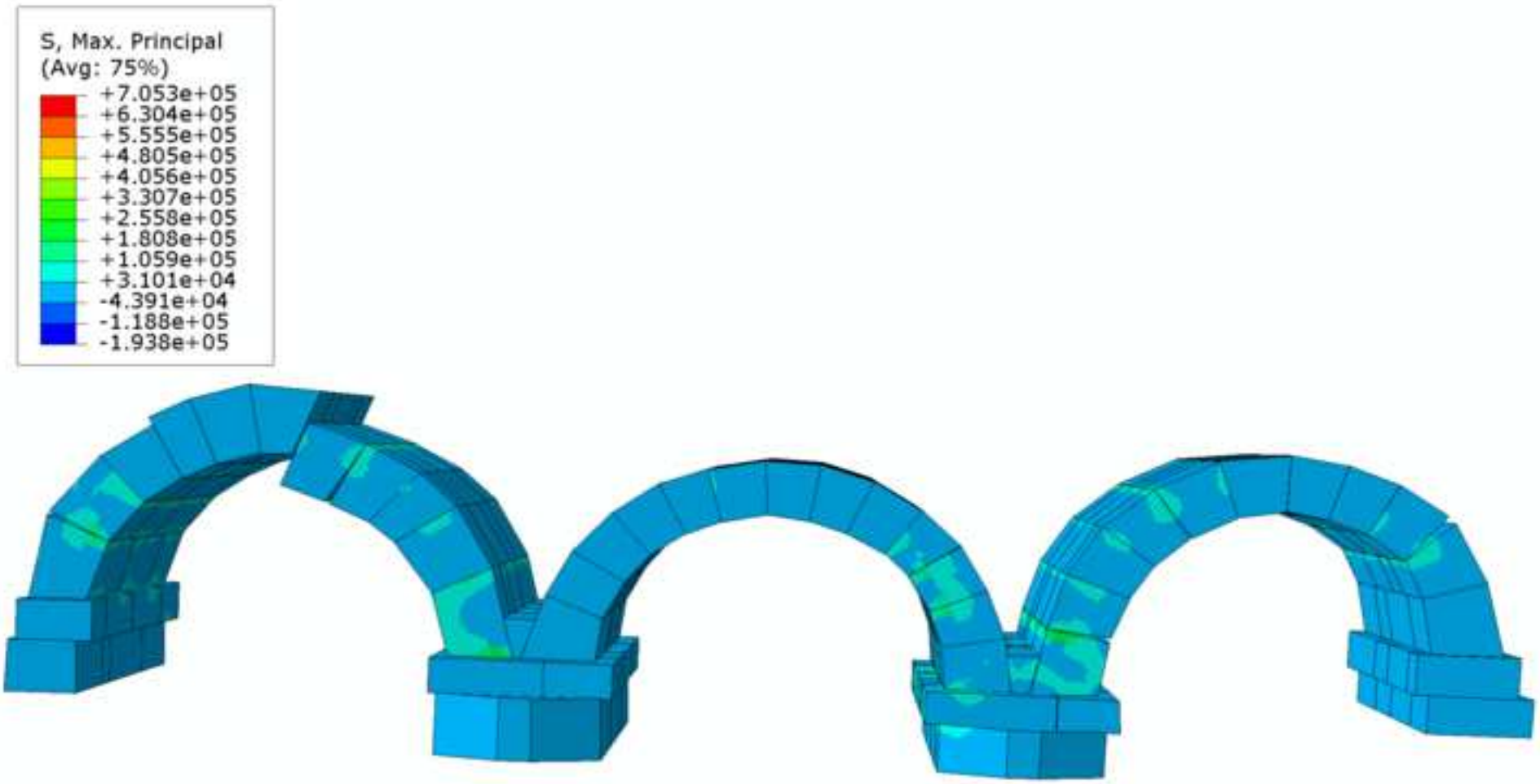

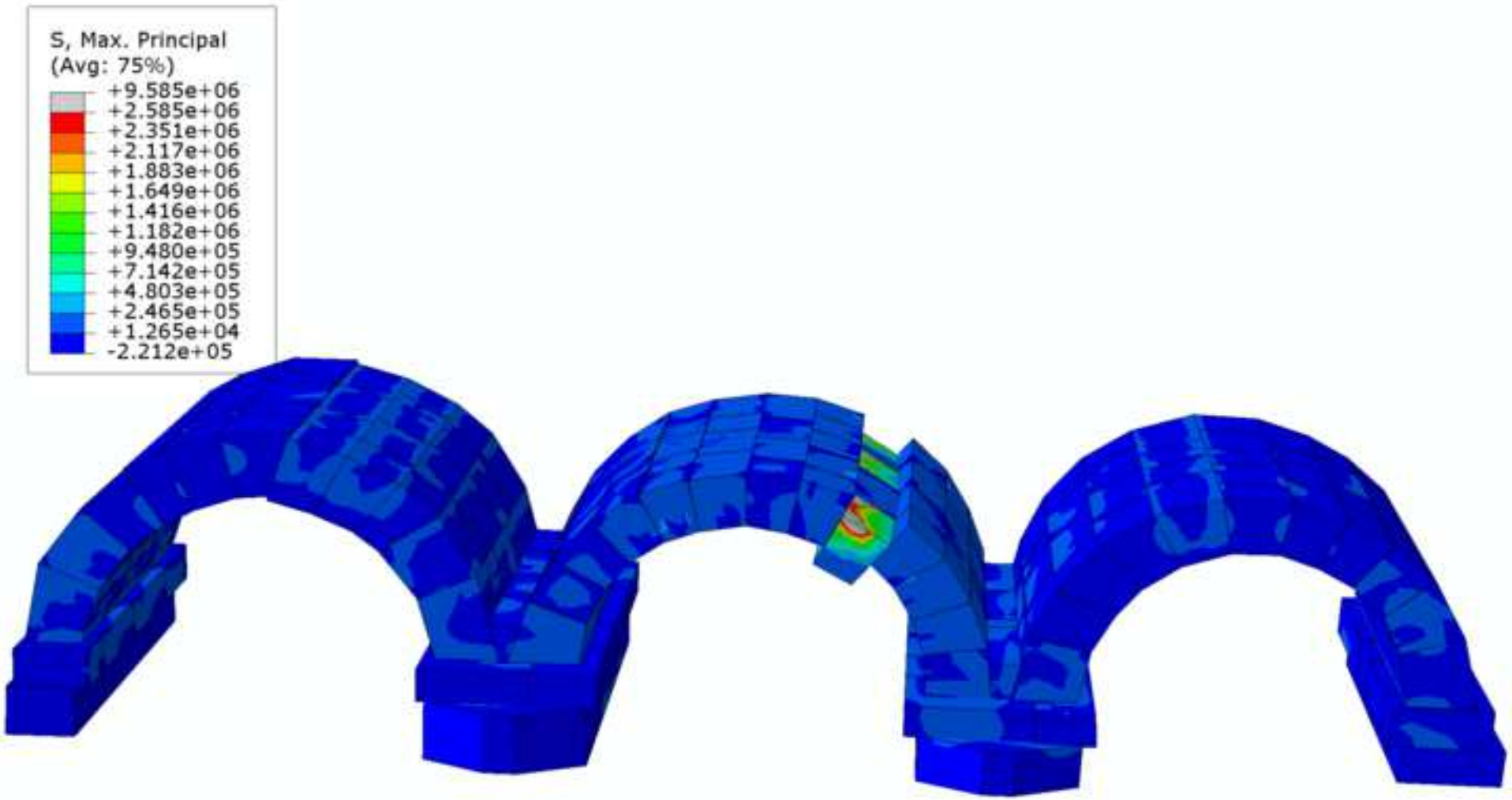

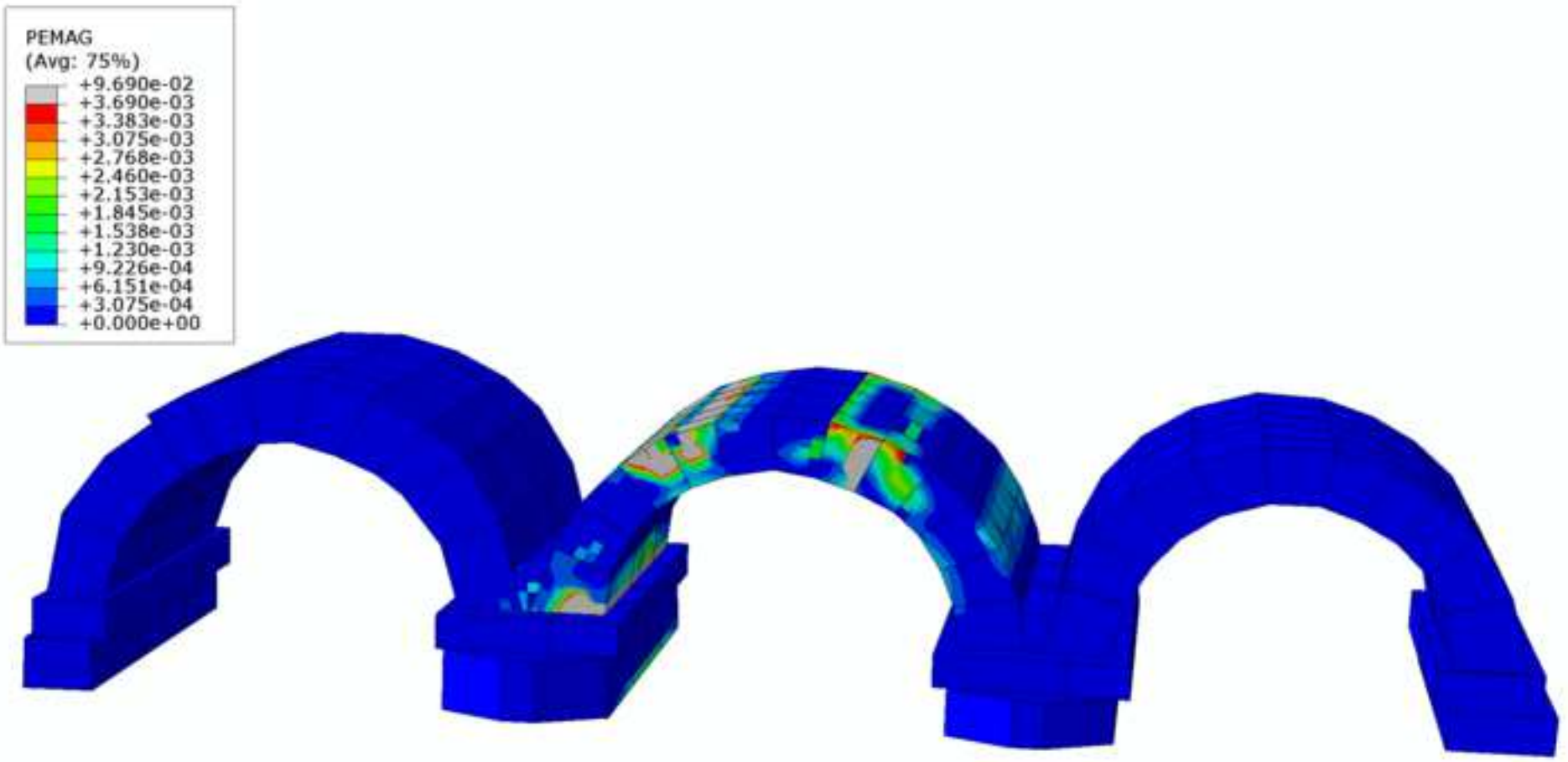

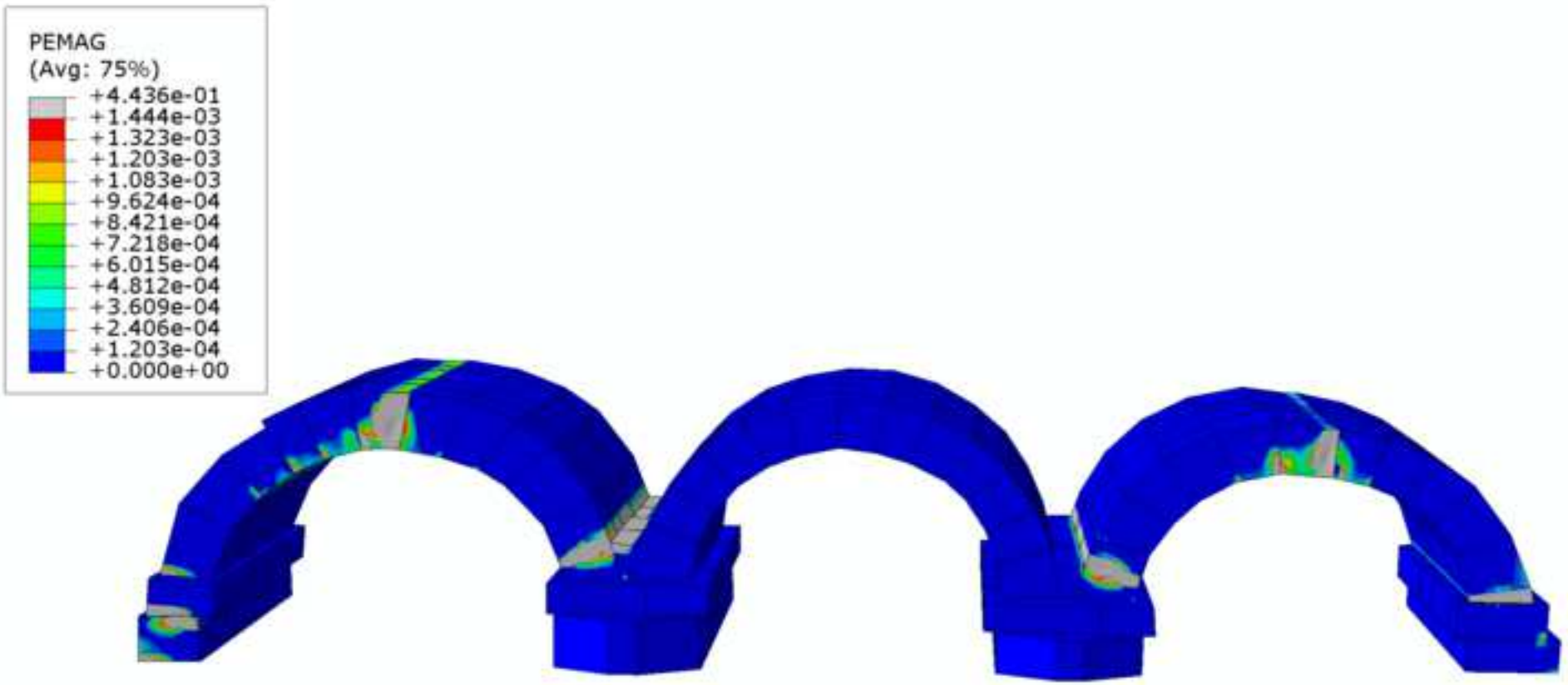

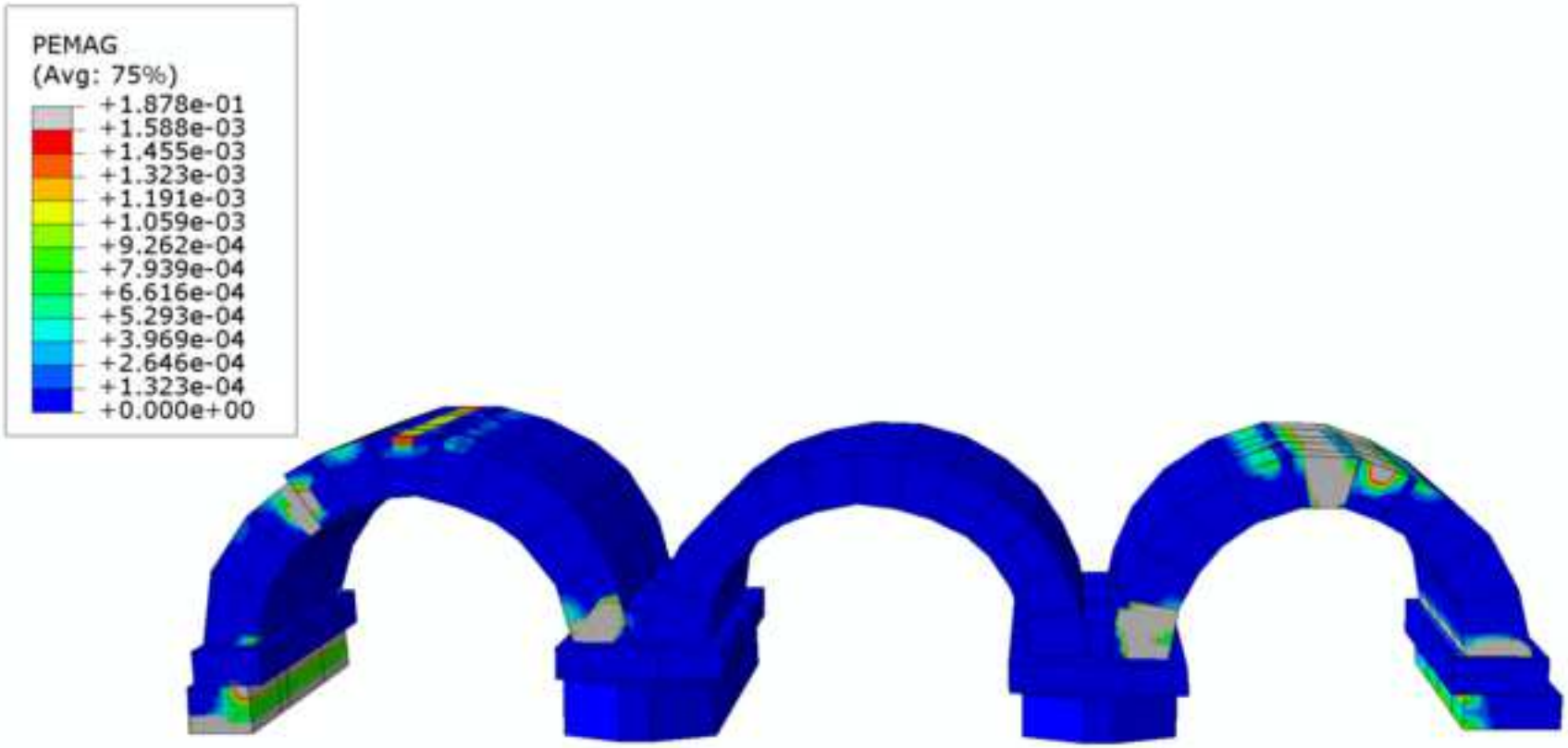

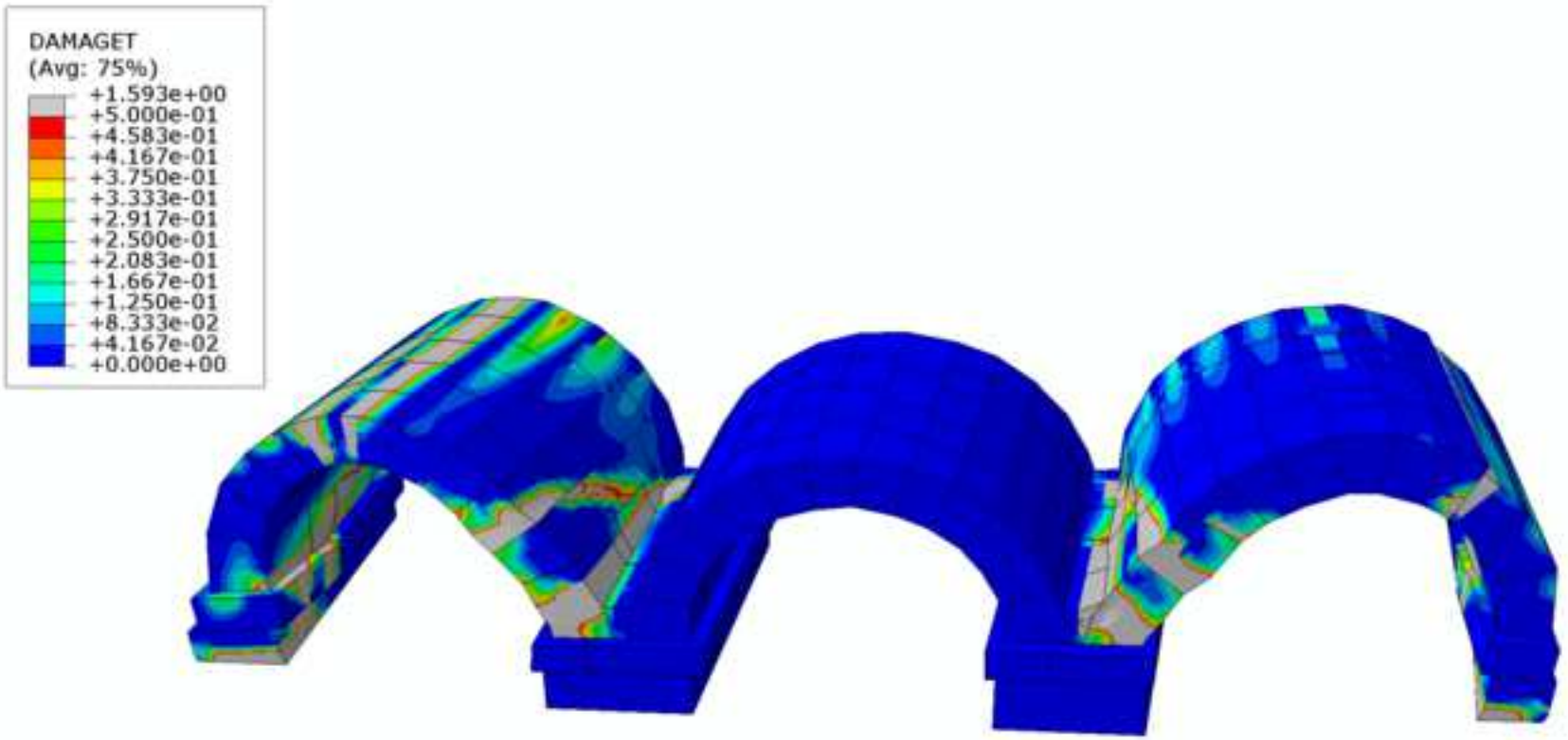

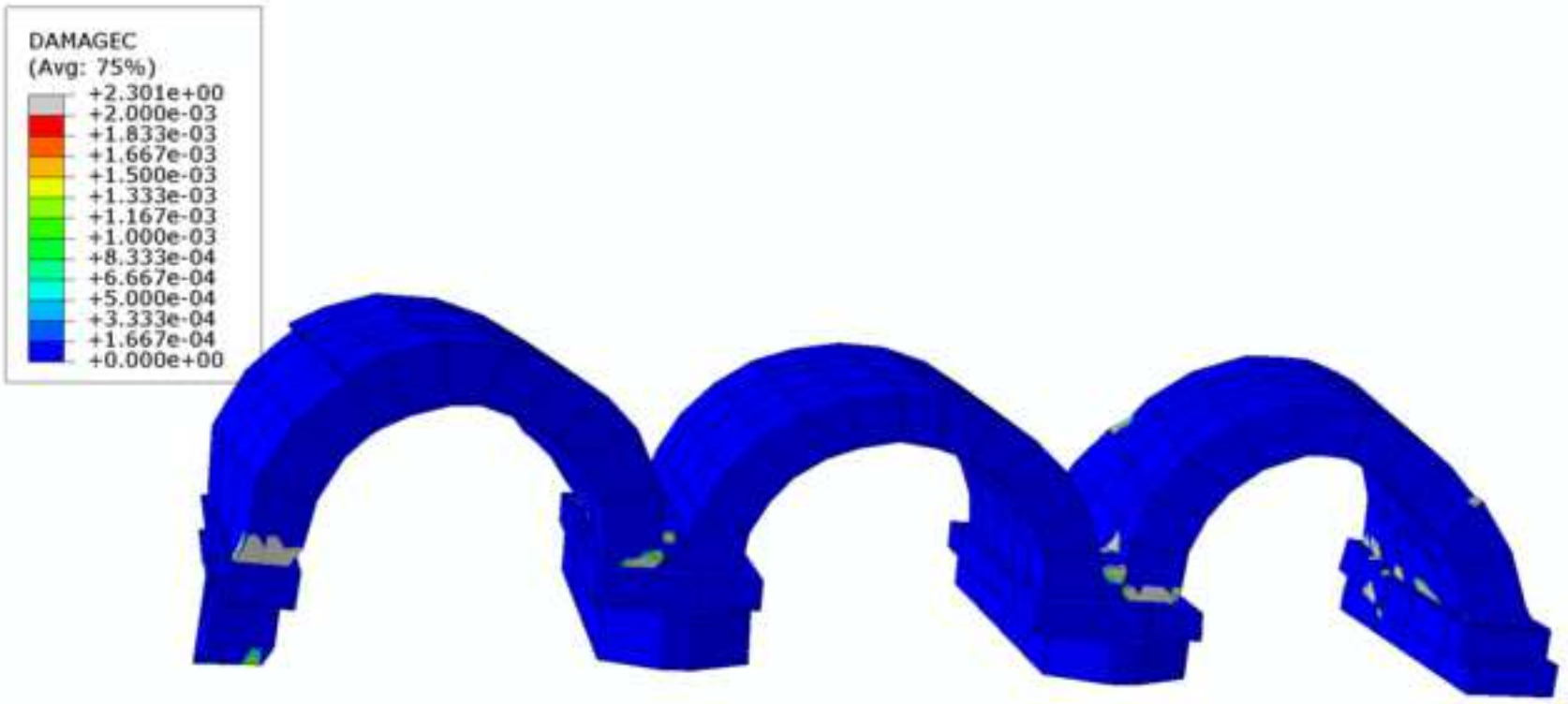

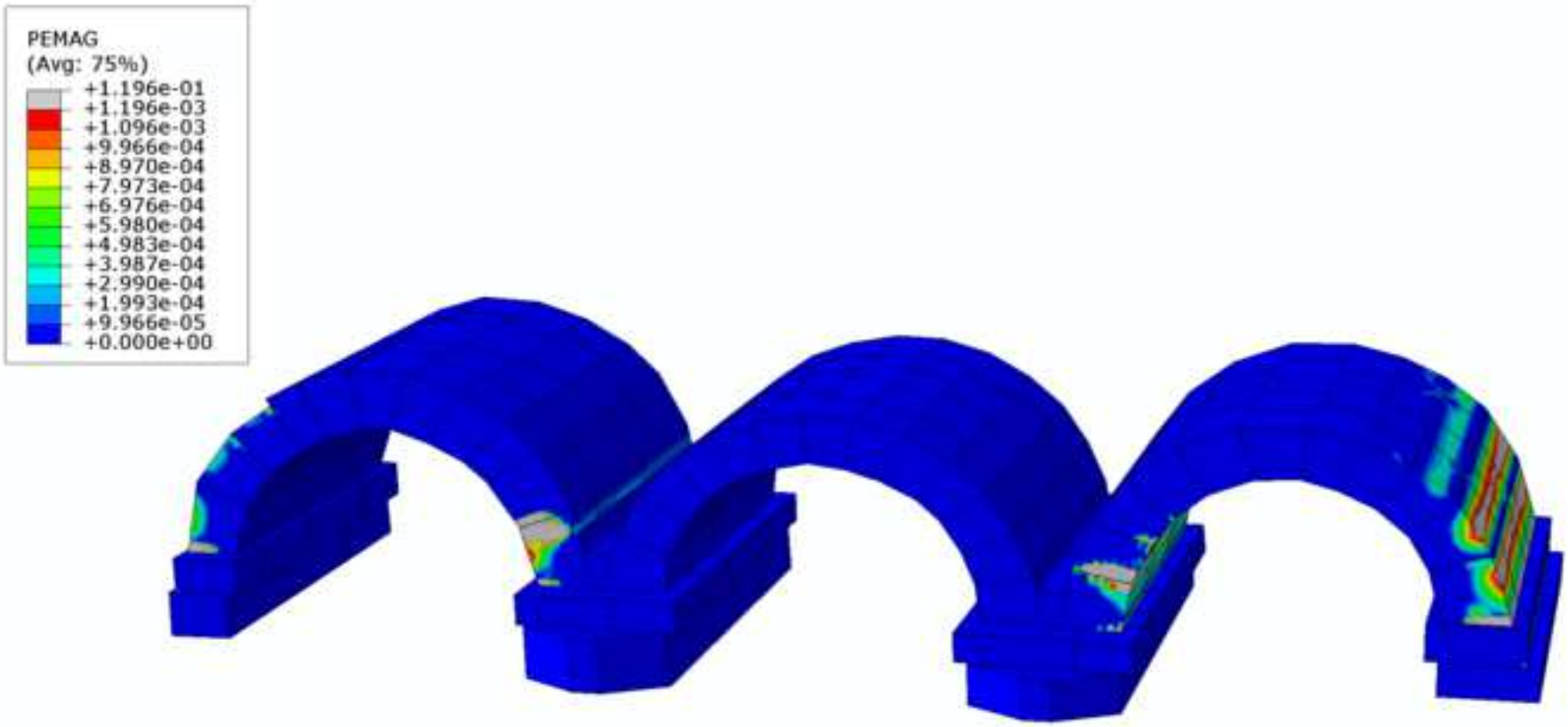

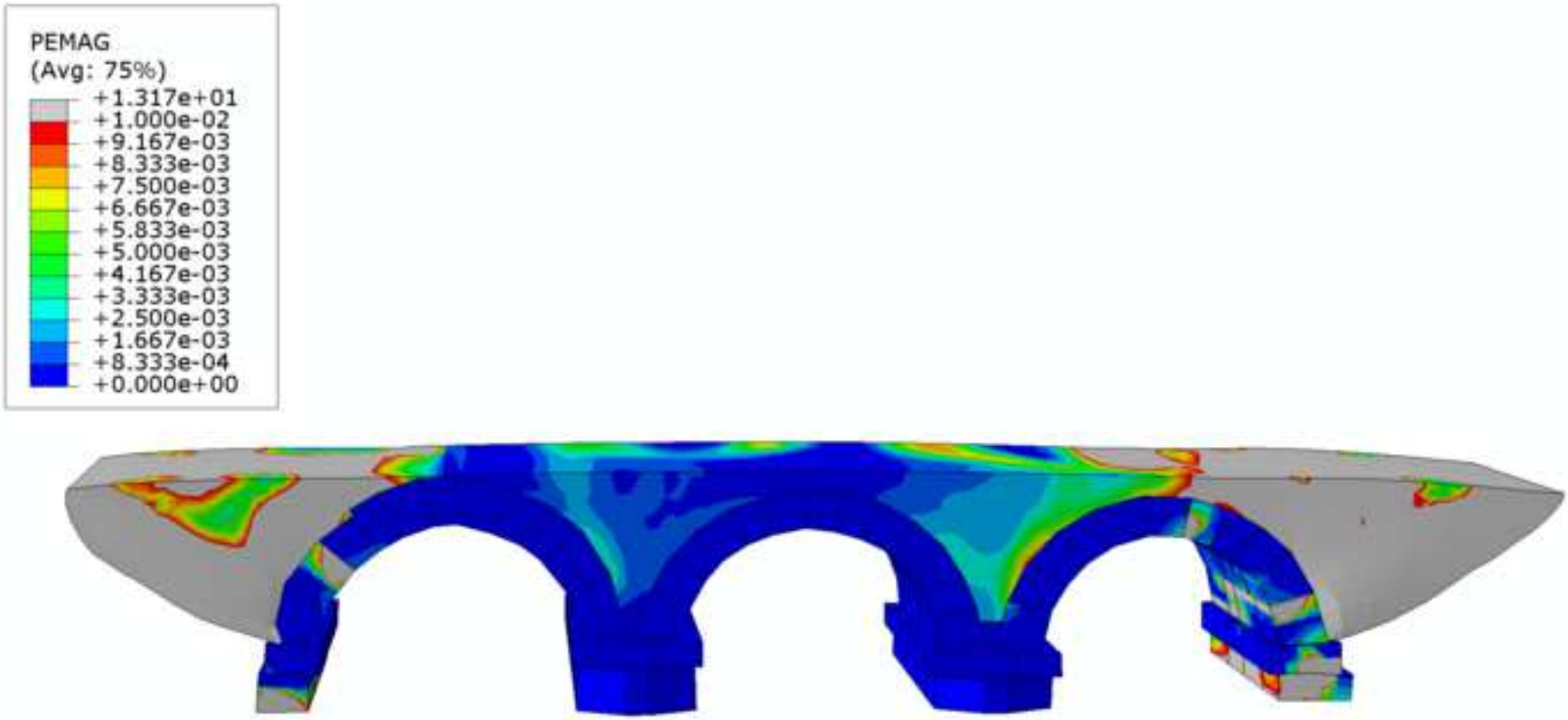

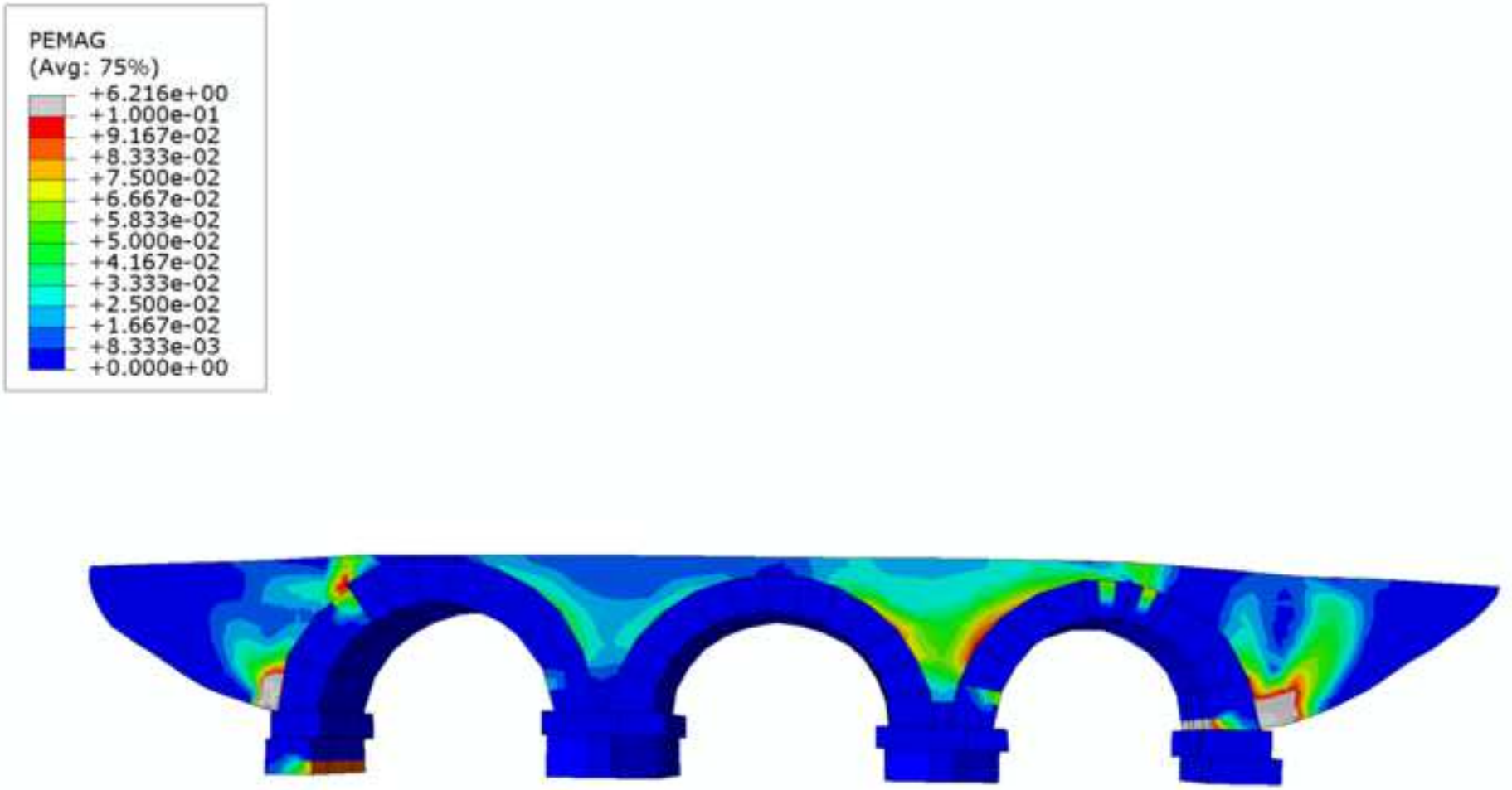

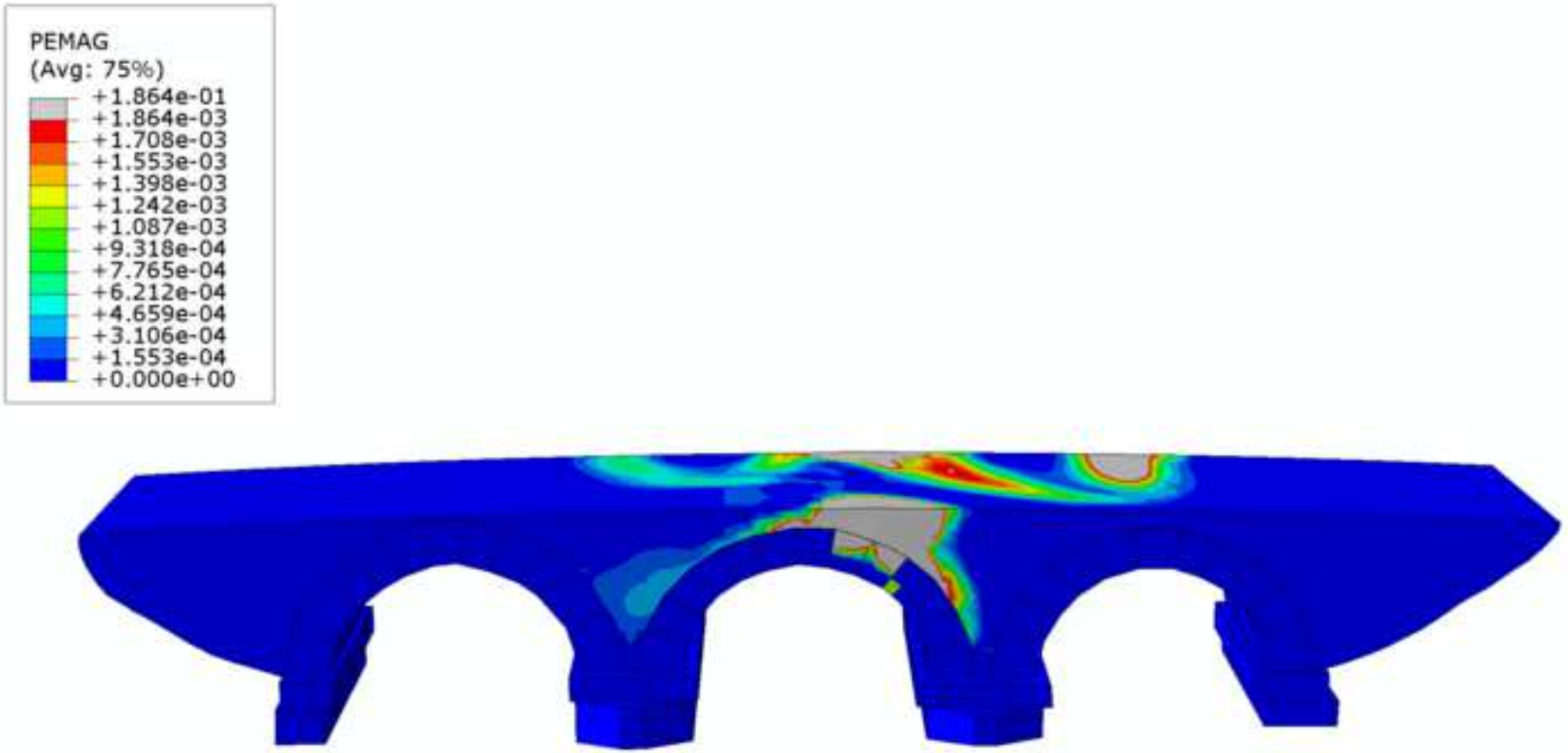

Figure

Click here to access/download;Figure;22.tif

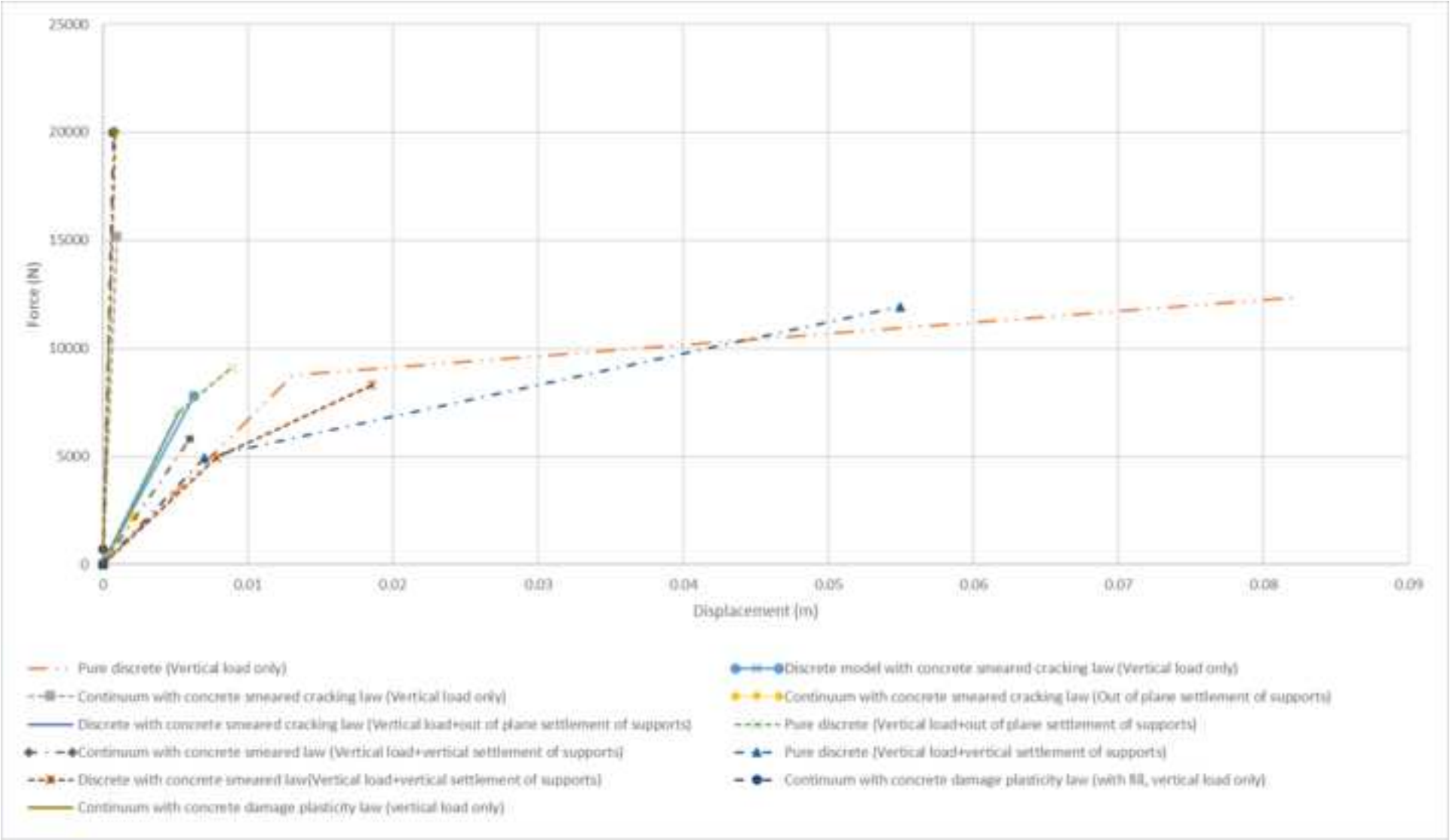

List of figures

Figure 9. Displacement (m) for inward horizontal settlements of the two outer supports (scale factor 3) for the discrete model with the concrete damage plasticity law.

Figure 10. Displacements (m) for out of plane settlements of the two inner supports (scale factor 5) for the discrete model.

Figure 11. Principal stresses (Pa) for downward settlements of the two inner supports (scale factor 5) for the discrete model.

Figure 12. Principal stresses (Pa) for downward settlements of the two inner supports (scale factor 5) accompanied by a vertical force at the middle arch, for the discrete model.

Figure 13. Plastic strain distribution developed in the concrete damage plasticity continuum model, for a vertical load applied at the quarter of the span of the middle arch.

Figure 14. Plastic strain distribution developed in the concrete damage plasticity continuum model, for outward horizontal settlement of the two outer supports.

Figure 15. Plastic strain distribution developed in the concrete damage plasticity continuum model, for inward horizontal settlement of the two outer supports.

Figure 16. Plastic strain distribution highlighting tensile damage developed in the concrete damage plasticity continuum model, for out of plane settlement of the two inner supports.

Figure 17. Plastic strain distribution highlighting compressive damage developed in the *concrete damage plasticity continuum model, for out of plane settlement of the two inner supports.*

Figure 18. Plastic strain distribution developed in the concrete damage plasticity continuum model, for downward settlement of the two inner supports.

Figure 19. Plastic strain distribution developed in the concrete damage plasticity continuum model with the backfill, for outward horizontal settlement of the two outer supports.

Figure 20. Plastic strain distribution developed in the concrete damage plasticity continuum model with the backfill, for inward horizontal settlement of the two outer supports.

Figure 21. Plastic strain distribution developed in the concrete damage plasticity continuum model with the backfill, for a vertical downward force applied on the backfill, in the position of the one quarter of the span of the middle arch.

Figure 22: Force-displacement diagrams for the discrete and the continuum models assigned a vertical downward load.